

Experimental Investigation of Mechanical and Electro-magnetic Behaviour of Lead-free Binary Solders with Trace Addition of Copper

by

Fahim Fazlullah

MASTER OF SCIENCE IN MECHANICAL ENGINEERING

STUDENT ID - 0417102011



Department of Mechanical Engineering

BANGLADESH UNIVERSITY OF ENGINEERING AND TECHNOLOGY

September 2021

The thesis titled “Experimental Investigation of Mechanical and Electro-magnetic Behaviour of Lead-free Binary Solders with Trace Addition of Copper” submitted by Fahim Fazlullah, Roll No: 0417102011, Session: April, 2017 has been accepted as satisfactory in partial fulfilment of the requirement for the degree of Master of Science in Mechanical Engineering on 12 September, 2021.

BOARD OF EXMINERS



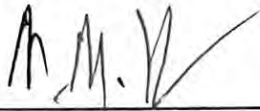
Dr. Shaikh Reaz Ahmed
Professor
Department of Mechanical Engineering
BUET, Dhaka-1000

Chairman
(Supervisor)



Dr. Shaikh Reaz Ahmed
Head
Department of Mechanical Engineering
BUET, Dhaka-1000

Member
(Ex-officio)



Dr. Muhammed Mahbubur Razzaque
Professor
Department of Mechanical Engineering
BUET, Dhaka-1000

Member



Dr. Mohammad Abdul Motalab
Professor
Department of Mechanical Engineering
BUET, Dhaka-1000

Member



Dr. Quazi Deen Mohd Khosru
Professor
Department of Electrical and Electronic Engineering
BUET, Dhaka-1000

Member
(External)

CANDIDATE'S DECLARATION

This is to certify that the thesis entitled, “Experimental Investigation of Mechanical and Electro-Magnetic Behaviour of Lead-Free Binary Solders with Trace Addition of Copper” is an outcome of the investigation carried out by the author under the supervision of Dr. Shaikh Reaz Ahmed, Department of Mechanical Engineering, Bangladesh University of Engineering and Technology, Dhaka-1000. This thesis or any part of it has not been submitted to elsewhere for the award of any other degree or diploma or other similar title.



Fahim Fazlullah

ACKNOWLEDGEMENTS

The author is deeply indebted and much obliged to Dr. Shaikh Reaz Ahmed, Professor, Department of Mechanical Engineering, Bangladesh University of Engineering and Technology (BUET), for his kind supervision and encouragement in carrying out this novel research as well as in writing this thesis. His profound knowledge and experience have made the successful completion of this comprehensive research possible.

The author is also grateful to Dr. M. S. Kaiser, Deputy Director of the Directorate of Advisory, Extension and Research Services, Bangladesh University of Engineering and Technology. for his help in various steps of sample preparation and measurement. The author is also grateful to the Departments of Glass and Ceramics Engineering, Electrical and Electronic Engineering, Materials and Metallurgical Engineering and the Department of Physics for providing laboratory facilities. Thanks, are also due to all the professors and staff of the Department of Mechanical Engineering, BUET for their cooperation and support.

ABTRACT

Lead-free solders are now-a-days of great practical importance, especially, for the electronic industries all over the world from both environmental and human health points of views. Several lead-free solutions for the solders are available in the industrial applications. Among these lead-free solutions, tin (*Sn*) based bismuth (*Bi*) and zinc (*Zn*) systems are the two main systems that are constantly being looked into for their superior performance. Aluminium (*Al*) is used as a minor alloying element on occasion. A new comparative analysis of the performances of three tin-based (*Sn*) potential lead-free binary systems, namely, *Sn-Bi*, *Sn-Zn* and *Sn-Al* with identical proportions ($Sn80\%x20\%$; $x = Bi/Zn/Al$) is conducted in the present thesis. More importantly, the effect of trace-addition (0~0.5% wt.) of copper (*Cu*) on the mechanical and electromagnetic characteristics of the binary solder systems is investigated along with their microstructural changes. For mechanical characterization, the tensile properties, microhardness and impact toughness are investigated. The bulk electrical conductivity, AC responses in terms of impedance, complex dielectric function and loss as well as complex permeability characteristics are studied for the purpose of electromagnetic characterization of the solder materials. The microstructure of the test alloys as well as their constituent elements is also investigated to explain the observed mechanical and electromagnetic behaviours. Optical micrographs and SEM images as well as EDS spectrum are included for this purpose.

Addition of trace-amount of copper causes formation of various intermetallic phases/compounds (IMC) in the tin-based systems, which is verified to have significant effects on mechanical as well as electromagnetic properties. Owing to the formation of IMCs and refining of the eutectic microstructures, the mechanical strength and hardness of the alloys increase as the *Cu* percentage increases, which are found to be in contrast with those of elongation and impact toughness characteristics. The electrical conductivity is found to improve up to a certain *Cu* composition; further increase in *Cu* decreases the conductivity due to excessive formation of IMCs and increased grain boundary area. By acting as electron scattering points, the intermetallic phases, however, negatively impact on the dielectric function and loss characteristics. Finally, from the comparison of characteristic behaviours of the present lead-free solder-alloy systems with those of traditional lead-solder (*Sn63Pb37*) as well as currently used lead-free solder (*SAC305*), it has been verified that the *Al* and *Zn*-based ternary alloy systems containing 0.3% *Cu* are highly promising candidates for lead-free solders in terms of their mechanical as well as electromagnetic performances.

TABLE OF CONTENTS

CANDIDATE’S DECLARATION	iii
ACKNOWLEDGEMENTS	iv
ABSTRACT	v
TABLE OF CONTENTS	vi
CHAPTER- 1: INTRODUCTION	1
1.1. Background	1
1.2. Scope of Current Research	2
1.3. Research Aim and Objectives	2
1.5. Structure of the Thesis.....	3
CHAPTER-2: LITERATURE REVIEW	4
2.1 Traditional Lead Solders.....	4
2.2 Lead-free Solders	5
2.3 Mechanical Properties of Solder Materials	5
2.3.1 Improvement of tensile characteristics	6
2.3.2 Creep behaviour.....	7
2.3.3 Wetting characteristics	8
2.3.4 Thermal conduction characteristics.....	9
2.3.5 Vibration and fatigue behaviour	9
2.4 Electro-Magnetic Properties of Solder Materials	10
2.4.1 Bulk conductivity.....	10
2.4.2 Solder joint conductivity	12
CHAPTER-3:MATERIALS AND EXPERIMENTAL DETAILS	14
3.1 Materials for Test Material Preparation	14
3.2 Test Material and Reference Solder Material Preparation.....	14
3.3 X-ray Fluorescence (XRF) Analysis	16
3.4 Preparation of Mechanical and Electrical Test Specimens	17
3.5 Mechanical Characterizations.....	20
3.5.1 Tensile test	20
3.5.2 Charpy impact test	21
3.5.3 Vickers hardness test.....	23
3.6 Electro-Magnetic Characterizations	24
3.6.1 Complex dielectric constant and loss tangent test.....	24
3.6.2 AC magnetic permeability test.....	25

3.6.3 Bulk conductivity test.....	25
3.7 Optical Microscopic Observation.....	26
3.8 Scanning Electron Microscope Observation	27
CHAPTER-4: MICROSTRUCTURAL OBSERVATIONS	28
4.1 Optical Microscopic Observations	28
4.2 SEM and EDS analysis.....	33
CHAPTER 5: CHARACTERIZATION OF MECHANICAL PROPERTIES	40
5.1 Stress-Strain Behaviour of the Alloys.....	40
5.2 Tensile Properties	43
5.3 Microhardness Characteristics.....	49
5.4 Impact Energy Characteristics	51
5.5 Comparison with Conventional Solders.....	53
CHAPTER- 6:CHARACTERIZATION OF ELECTROMAGNETIC PROPERTIES	58
6.1 Electrical Conductivity.....	60
6.2 AC Dielectric Characteristics	64
6.3 AC Magnetic Characteristics	70
6.4 Estimation of Thermal Conductivity of the Solder Materials from Bulk DC Conductivity	74
6.5 Comparison with Commonly used Solders	77
CHAPTER-7: CONCLUSIONS AND RECOMMENDATIONS	79
7.1 Conclusions	79
7.2 Recommendations	80
REFERENCES.....	82
Appendix A	1
Characterization of Traditional Lead Solder with Compositional Variation	A-1
A.1 Background	A-1
A.2 Mechanical Characterization	A-1
A.3 AC Electrical Characterization.....	A-5
A.4 Bulk Conductivity	A-10
A.5 AC Magnetic Characterization	A-10
A.6 Microstructure Observations.....	A-12

LIST OF FIGURES

Figure 3. 1 Photographs of (a) Casting die (b) Preparation of the samples	15
Figure 3. 2 Drawings of Mechanical and Electrical test specimens with dimensions: (a) Tensile specimen, (b) Impact Test specimen, (c) AC and Bulk conductivity specimen and (d) AC Magnetic specimen.....	19
Figure 3. 3 Actual Photographs of Mechanical, Electrical and Magnetic Test sample images	20
Figure 3. 4 Tensile Tester	21
Figure 3. 5 Charpy Impact Test Angles.	22
Figure 3. 6 Charpy Impact Tester	22
Figure 3. 7 (a) Impedance Analyzer (b) Equivalent circuit model for dielectric characteristics	24
Figure 3. 8 (a) Wound toroid sample (b) equivalent circuit	25
Figure 3. 9 Micro-ohmmeter.....	26
Figure 3. 10 Optical microscope.....	26
Figure 3. 11 Scanning electron microscope.....	27
Figure 4. 2 Photomicrographs of Sn-Bi material system with trace addition of Cu: (a) Sn- 20wt%Bi, (b) Sn-19.9wt%Bi-0.1%Cu, (c) Sn-19.7wt%Bi-0.3%Cu, (d) Sn-19.5wt%Bi- 0.5%Cu	30
Figure 4. 3 Photomicrographs of Sn-Al material system with trace addition of Cu: (b) Sn- 20wt%Al (e) Sn-19.9wt%Al-0.1%Cu, (b) Sn-19.7wt%Al-0.3%Cu (e) Sn-19.5wt%Al- 0.5%Cu	31
Figure 4. 4 Photomicrographs of Sn-Zn material system with trace addition of Cu: (a) Sn- 20wt%Zn (b) Sn-19.9wt%Zn-0.1%Cu, (c) Sn-19.7wt%Zn-0.3%Cu (d) Sn-19.5wt%Zn- 0.5%Cu	32
Figure 4. 5 SEM and EDS analysis of Sn ₂₀ Bi sample	34
Figure 4. 6 SEM and EDS analysis of Sn _{19.90} Bi _{0.5} Cu sample	35
Figure 4. 7 SEM and EDS analysis of Sn ₂₀ Al sample.....	36
Figure 4. 8 SEM and EDS analysis of Sn _{19.90} Al _{0.5} Cu sample	37
Figure 4. 9 SEM and EDS analysis of Sn ₂₀ Zn sample	38
Figure 4. 10 SEM and EDS analysis of Sn _{19.90} Zn _{0.5} Cu sample.....	39
Figure 5. 1 Effect of Cu addition on the stress strain behaviour of the three binary solder systems(a) 0% wt. copper (b) 0.1% wt. copper (c) 0.3% wt. copper (d) 0.5% wt. copper	42
Figure 5. 2 (a)Mechanical Strength (Tensile Strength) of the three binary solder alloy systems, (b) Effect of Cu-addition on Tensile Strength	44
Figure 5. 3 (a) Elongation at break of the three binary solder alloy systems, (b) Effect of Cu- addition on Elongation at break.....	46
Figure 5. 4 (a) Elastic modulus of the three binary solder alloy systems, (b) Effect of Cu- addition on elastic modulus.	48
Figure 5. 5 (a)Microhardness of the three binary solder alloy systems, (b) Effect of Cu- addition on microhardness.....	50
Figure 5. 6 (a) Impact energy of the three binary solder alloy systems, (b) Effect of Cu- addition on impact energy	51

Figure 5. 7 Comparison of major mechanical properties of the lead-free solder materials (with 0.3% Cu addition) with conventional SAC305 and Sn63Pb37 solders: (a) Tensile strength, (b) Elongation at break, (c) Microhardness, (d) Elastic Modulus, (e) Impact Energy, (f) Thermal Conductivity	57
Figure 6. 1 (a) Bulk DC conductivity of the constituent elements and the binary alloys, (b) Change in conductivity with copper content	59
Figure 6. 2 Frequency response of dielectric Properties of the constituent pure elements and binary alloys :(a-c) Dielectric Constant plots of Sn-Bi, Sn-Zn &Sn-Al binary alloys respectively, (d-f) Dielectric Loss plots of Sn-Zn &Sn-Al binary alloy	62
Figure 6. 3 Frequency response of dielectric Properties: (a) Dielectric Constant at 0% wt. Cu (b) Dielectric Constant at 0.1% wt. Cu (c) Dielectric Constant at 0.3% wt. Cu (d) Dielectric Constant at 0.5% wt. Cu	63
Figure 6. 4 Frequency response of dielectric Properties: (a) Dielectric Loss at 0% wt. Cu(b) Dielectric Loss at 0.1% wt. Cu (c) Dielectric Loss at 0.3% wt. Cu (d) Dielectric Loss at 0.5% wt. Cu.	64
Figure 6. 5 Impedance vs frequency plots of the constituent elements and the binary alloys: (a)Sn-Bi alloy, (b)Sn-Zn alloy, (c) Sn-Al alloy.....	68
Figure 6. 6 Impedance vs frequency of the alloy samples: (a) 0 % wt. Cu (b)0.1% wt. Cu (c) 0.3% wt.Cu (d) 0.4% wt. Cu.....	69
Figure 6. 7 Frequency response of the relative permeability of the constituent elements and the corresponding binary alloys.....	71
Figure 6. 8 Frequency response of relative permeability of the solder alloy systems: (a) Real part 0.3% wt. Cu (b) Imaginary part 0.3% wt. Cu (c) Real part 0.5% wt. Cu (d) Imaginary part 0.5% wt. Cu.....	73
Figure 6. 9 Comparison of electrical characteristics of the solder samples with those of conventional solders	77
Figure 6. 10 Comparison of permeability characteristics of the solder samples with those of conventional solders	78

LIST OF TABLES

Table 4. 1 Chemical composition of the raw ingots used.....	14
Table 4. 2 Chemical composition of the binary and ternary alloys	16
Table 4. 3 Chemical composition of the reference solder materials.....	17
Table 4. 4 Dimensions of tensile test specimen.....	18
Table 4. 5 Charpy Test Parameters and Their Standard Values	23
Table 5. 1 Measured and recorded values of mechanical properties of the reference alloys ..	53
Table 5. 2 Hardness and Tensile Properties of the Experimental Alloys	55
Table 5. 3 Impact Energy and Thermal conduction characteristics of the Experimental Alloys	56
Table 6. 1 Chemical composition of the raw ingots used.....	74

CHAPTER- 1

INTRODUCTION

1.1. Background

With rapid growth of modern electronics industry, devices such as smartphones, personal computers and other digital devices have become a part of daily life. These devices are used in every facet of modern life from the manufacturing industry to the medical field and also in conducting various scientific researches. With such permeance of these devices, electronic waste produced after the expiration of lifetime is great problem. If left unaddressed waste from such sources can cause irreversible damage to the environment. Recycling is one way of reducing such waste but, there are difficulties associated with that as well. It takes considerable number of resources, time and suitable facilities to recycle such electronic waste. And as a result, it often becomes too expensive and thus impractical to recycle such waste. Yet these elements such as cadmium, lead, lithium etc. cannot be left in landfills as the chance of harm to human and wildlife is high. One way to counter such possibly dangerous situations is to reduce the use of such toxic elements or to find suitable alternatives to such elements. Many researchers around the world are currently looking for such alternatives. Particularly one case among these sources of e-waste is of interest in this current research. That is the element used in most common solder alloys, lead (Pb). Even now lead is used almost ubiquitously for most electronics applications. For this reason, there has been numerous investigations to find alternatives for lead in solder alloys.

Conventional lead-tin alloys are so widespread because of their low melting point, good wettability, low cost, good electrical conductivity and satisfactory mechanical characteristics such as strength and ductility for most electronic applications. Any suitable alternatives to the conventional solder have to at least match these characteristics if not exceed them. Numerous alternatives have been proposed and studied so far, these include bismuth (Bi) alloys, zinc (Zn) alloys and gold (Au) based solders. Trace elements such as copper (Cu), silver (Ag), nickel (Ni) have been added to improve the characteristics of said alloys these alloys. One alternative of conventional solders is the SAC solder family primarily containing tin and silver with trace amounts of copper.

However, elements such as gold, silver and copper are expensive. Then, there is the issue of availability as well. As these materials are not always easily available.

1.2. Scope of Current Research

This research aims to find a suitable replacement for conventional tin-lead based alloys. In order to accomplish this, it is necessary that all the previous work on this matter be studied and brought together, which has so far not been done. Individual alternatives such as tin-zinc system, tin-bismuth system has been studied in great detail but, there is a lack of a holistic research comparing different alternatives on the basis of their characteristics. In order to accomplish such goal three lead substitutes bismuth, zinc and aluminium were chosen at a specific composition with tin and their mechanical properties were analysed.

Research on the electrical characteristics of different solder alloys systems has also been carried out extensively in the past but, this research has usually for the most part been conducted separately in relation to mechanical properties. Also, the most extensively studied electric property has usually been the bulk (DC) conductivity. While their AC electric properties namely dielectric properties relating to energy loss, storage has not been studied at all due to the difficulties associated with such investigations. In this regard the current investigation differs heavily from past investigations, in that, it aims to not only compare the lead alternatives on the basis of their mechanical, DC conductive and AC electrical characteristics. An attempt has also been made to link these properties to the microstructure of the materials.

1.3. Research Aim and Objectives

The current study has two targets. The first is to fill a gap in the literature by undertaking a thorough evaluation of solder materials from both mechanical and electrical perspectives. The other is to compare and contrast few selected potential solder materials based on all of their essential mechanical and electrical features in order to identify feasible alternatives to traditional solders.

The main aim of this research is to find one or more suitable alternatives among Sn-Bi, Sn-Al and Sn-Zn to conventional solders. If no single alternative is best suitable for replacement of conventional Sn-Pb system, then the aim is to find which of the systems comes closest, and identify in which areas they fall behind. The secondary goal is to find

out what areas do the individual systems excel at. For example, one system may be suitable for lower temperature soldering, while another excels at high temperature solder applications, yet another may be specially suited for soldering application where the components are subjected to prolonged periods of moderate loads due to its inherent toughness. It is also a special aim of this research to investigate the AC current characteristics, more specifically the dielectric characteristics as there is a significant lack of knowledge. With all that said the specific objectives of the research are:

- I. Investigation of major mechanical and electro-magnetic properties of practical interest for a number of Tin based lead-free binary solders.
- II. Identification of possible variation in mechanical as well as electro-magnetic behaviour of the above binary solders with trace addition of copper.
- III. Selection of suitable lead-free alternative(s) to traditional Sn-Pb solders through a comparative analysis of major behaviours/performances in relevant fields of interests.

1.5. Structure of the Thesis

The structure of the current thesis is as follows-

- I. **Chapter 1** gives some important background information, highlights the scope of the study as well as the motivation and objectives of the current investigation.
- II. **Chapter 2** is a revisit of previous works in the field of solder alloy development.
- III. **Chapter 3** is a detailed description of the methodology involving this research
- IV. **Chapter 4** is the microstructure observations conducted using optical and scanning electron microscope.
- V. **Chapter 5** is the analysis of the mechanical properties of the experimental solder alloy
- VI. **Chapter 6** details the analysis of AC and DC properties of the alloys.
- VII. **Chapter 7** marks some of the key take aways from this current research & discusses what can be done in future regarding solder alloys based on current observations.

CHAPTER-2

LITERATURE REVIEW

2.1 Traditional Lead Solders

The usage of pure tin as soldering alloy dates back to around 4000 years ago. Its first use was around the Mediterranean when the Cretans showed it to the Etruscans, who later went on to teach it to the Romans, Tunisians and Spanish, followed by many others.

Tin itself has excellent properties that make it ideal for soldering. Especially its low resistivity [1] and good wettability [2]. However, there are two main problems that inhabit the use of pure tin as soldering material. First is tin pest and the second is tin whiskers. At low enough temperatures (13°C or lower) white α -Sn having diamond structure transforms into grey β -Sn with body-centered tetragonal structure [3,4]. β -Sn being brittle and non-conductive creates problems in colder climates. Tin whiskering is the more serious of the two problems. Tin whiskers are electrically conductive, crystalline tin formations that can form on surfaces where tin is employed as a final finish. Tin whiskers have been seen to grow to lengths of several millimetres (mm), and in some cases to lengths of more than ten millimetres (mm). Short circuits induced by tin whiskers have been blamed for a slew of electronic system failures [5].

Both of these problems are what lead to the development of conventional tin-lead solder. Lead is especially effective in suppressing tin whiskers. Lead-tin solders particularly the eutectic 63Sn-37Pb have been extensively used as interconnects for this particular reason. In addition, lead-tin solders are also cost effective and excellent for low temperature soldering. Good wetting characteristics [6], electrical and thermal conductivity [7] and good tensile strength [8] has also attributed to its wide spread adoption as well. They are also used in high melting temperature type solders as well due to high thermal cycling reliability [8]. While lead free alternatives are now the subject of focus, research on conventional lead alloys for some specific applications is still on going. One such sector is the soldering of aluminium alloys which are used in aerospace and automotive industry [9,10]. With the miniaturization of electronic components and the development of a multi-step assembly process, low melting point solder alloys have become necessary for temperature-sensitive devices, Sn-Pb-Cd alloys have shown promise in this regard. Research is ongoing to improve the mechanical properties of Sn-Pb-Cd alloys [11,12].

2.2 Lead-free Solders

Lead-free solder alloys have been present for as long as people have soldered, with 5000-year-old sources. The majority of these alloys were copper-silver or silver-gold alloys that were employed in so-called hard soldering. This method of soldering precious and semi-precious metals is still utilized today.

In modern times phasing out of lead (Pb) as well as new requirements for increasingly more fine-pitched components in electronics industry has led to the development of new solder alloys that can fill this role. In 2006 when the deadline for When the deadline for implementation of the RoHS legislation was approaching, Sn-Ag-Cu eutectic and Sn-Cu eutectic were chosen as the alternatives for conventional Sn-Pb alloys. However, the expense of the Iowa State University patent [13] caused the Japan Electronic Industry Development Association to recommend the hypoeutectic SAC305 alloy, which was then covered by a Japanese patent held by Senju Metal Industries (patent no. 3027441). SAC305 has a lower melting point (217 °C) than most Sn-Cu alloys, which have a higher melting point (227 °C); and SAC305 performs similarly to high-Ag Sn-Ag-Cu eutectic but is less costly [14]. As a result, the IPC's decision to approve SAC305 as solder of choice for the electronics sector [14]. Other lead-free solders include the Sn-Bi, Sn-Zn, Zn-Al (high temperature solder) & Au-Sn (high temperature solder) alloys [15-17]. These alloys have been modified with the addition of various trace elements such as Cobalt (Co), Chromium (Cr), Nickel (Ni), Iron (Fe), Manganese (Mn), Silicon (Si), Titanium (Ti), Palladium (Pd), Platinum (Pt), Germanium (Ge), Cadmium (Cd), Indium (In) etc. [14]. One other popular method of improving the properties (both mechanical and electrical) of lead-free solders is the incorporation of carbon nanotube into the alloys [18-20].

2.3 Mechanical Properties of Solder Materials

A few of the important mechanical properties of solder alloys include, their tensile characteristics, creep behaviour, wetting characteristics, thermal conduction characteristics, vibration and fatigue characteristics of the solder materials. In regards to these properties, recent investigations are highlighted in the following section.

2.3.1 Improvement of tensile characteristics

In terms of improving strength, McCormack, Jin, Kammlott and Chen found that adding a small amount of zinc significantly improves the mechanical strength of Sn-3.5%Ag alloy while maintaining the same level of ductility. Their investigation showed that the improvement was almost 48%. This strengthening from the Zn additions is attributed to a substantial refinement of the precipitates in the solidification microstructure. By just adding 0.5 % Zn the strength improves significantly from 8 Ksi to almost 12 Ksi with marginal decrease in ductility. The best result was found at 1% Zn composition, where the Sn dendrite formation is almost completely suppressed with uniform microstructure. These grains are finely dispersed with small Ag₃Sn precipitates [21]. Kariya and Otsuka studied the effects when instead of zinc, bismuth was added to the Sn-3.5%Ag alloy. They found that adding bismuth dramatically reduced fatigue life while increasing tensile strength. In addition, there was also an observed decrease in ductility [22]. Presence of bismuth up to 2% slightly changes the microstructure of the alloy. Slightly smaller β -Sn globules and irregularly shaped (coarse and plate like) Ag₃Sn around β -Sn globules are seen in comparison with binary Sn-3.5Ag alloy causing the increased strength and decreased ductility and fatigue behaviour [22]. Chen, Lee and Yip studied the mechanical properties and intermetallic compound formation at Sn/Ni and Sn-0.7wt.%Cu/Ni joints. They found that the thickness of the intermetallic compound layers grows, while the joint strength decreases with longer reaction time [23]. The solder joint strength is closely related to the growth of the compounds. Quan, Frear, Grivas and Morris observed this while studying Sn-Pb/Cu joints. They found that for 60Sn-40Pb alloy there was a decrease in strength due to the thicker Cu₆Sn₅ layer and the coarser grains of the Cu₆Sn₅ intermetallic at the alloy-Cu solder joint. Adding 2% In/Ag/Sb/Bi decreases Sn availability for Cu-Sn intermetallics, resulting in thinner Cu-Sn intermetallic layers resulting in improved strength [24]. Islam, Wu, Chan and Jillek made investigations into the microhardness of Sn-Zn based alloys. They also examined the effect of cooling rate on hardness. It is found that with increasing reflow temperature the hardness of Sn-9Zn and Sn-37Pb decreases due to the fact that larger grains were formed at higher temperature; especially Sn-9Zn shows a gradual decrease in hardness with increasing temperature. In contrast, the microhardness of Sn-8Zn-3Bi increases with increasing temperature due to segregation of a hard-Bi rich phase in the structure [25]. Sn-Ag-Cu composite solders reinforced with nano-sized, nonreacting, no coarsening 1 wt% TiO₂

particles were created and their hardness and thermal behavior were analyzed by Gain, Chan and Yung. Addition of the TiO_2 nano particles gave the Sn-Ag-Cu alloy higher hardness due to well controlled and homogeneous distribution of TiO_2 nano-particles [26]. Yang et al studied the effects of Ni addition to Sn58Bi alloys [27]. The results indicate that the elastic modulus, tensile and yield strength increase with the increasing Ni content during the solid-state aging, which is because Ni can decrease the CTE and refine the microstructure of SnBi solder. The ductility of composite solders presents a non-monotonic trend with the increasing Ni content and aging time because the concentrated Ni_3Sn_4 grains form at the solder matrix [27].

2.3.2 Creep behaviour

Another important characteristic of any solder alloy is its creep behaviour, and the relation of this creep behaviour to microstructural features and external factors like cooling rate, cooling time etc. And as a consequence, a lot of work has been done regarding this matter. The relation between creep and temperature dependence for Sn-Ag-Cu lead-free solder was studied by Han et al [28]. They found that as the temperature increased, the creep response also increased. The hardness of the Sn-3.5Ag-0.7Cu solder was also observed to decrease with increasing temperature due to the softening effect [28]. lead-free SAC solder joints have a coarse-grained microstructure with only a few large anisotropic Sn grains throughout the joint after reflow. Within each grain, the proeutectic Sn is mostly in dendritic form, with the space between the dendritic lobes filled in with a eutectic Sn–Ag phase that consists of nanoscale Ag_3Sn intermetallic compounds (IMCs) present in a Sn matrix. In addition, there are micron-scale Cu_6Sn_5 IMC precipitates with either straight or branched rod like structures of hexagonal cross section, mostly present at Sn dendrite boundaries and grain boundaries, which obstruct grain-boundary sliding [29]. Sn phase in SAC alloys can solidify in different morphologies depending on the solidification conditions (e.g., cooling rate) and the metallurgical conditions that are governed by the nominal composition of the solder and the metallization on the printed wiring board and components [30]. Varying the Ag content in SAC alloys contributes to varying volume fraction of pro-eutectic Sn dendrites versus the eutectic phase and also affects the size and distribution of nanoscale Ag_3Sn intermetallic precipitates within the eutectic phase [31].

2.3.3 Wetting characteristics

Wettability of solder alloys is also an important characteristic since it determines the final quality of the solder joint. It is the ability of a liquid metal/alloy to spread over a solid surface [32]. It is well established that wetting plays a major role in the formation of a metallurgical bond at the solder– substrate interface, describing the extent of intimate contact between a liquid and solid [33]. The driving force behind this mechanism is due to the interfacial energy resulting from an imbalance of the surface and interface energies [34]. Sona and Prabhu studied the effect of Reflow Time on Wetting Behaviour, Microstructure Evolution, and Joint Strength of Sn-2.5Ag-0.5Cu Solder. According to them, wettability was assessed by measuring the equilibrium contact angle. However, it was well known that interfacial reactions take place immediately when liquid metal contacts the substrate. Hence, a correlation between the equilibrium contact angle and joint strength may be misleading, particularly in the case of reactive systems; Under such circumstances, spreading kinetics has to be considered. Therefore, they focused on the study of the wetting kinetics of Sn-2.5Ag0.5Cu on bare and Ni-coated Cu substrates, the interfacial reaction at the solder–substrate interface, and the corresponding joint strength as a function of reflow time, using a novel quench setup to obtain precise control over reflow time [35]. Rodrigues et al took a different approach in that they measured and modelled the contact angle SAC 305 solder. They found that it was possible to accurately predict the shape of the melted solder and, this way, complement the experimental measurements by means of numerical approach. Also, results proved that increasing the surface tension value did not have a high influence on the solder shape. On the other hand, increasing the contact angle, while keeping a value for the surface tension according with the literature, allowed a better shape approximation to the experimental results [36]. Sharma, Sohn and Jung tried to modify the wetting behaviour of Sn-3.0Ag-0.5Cu (SAC) alloy by adding graphene Nanoplatelets. The experimental results indicated that an addition of 0.05 wt pct GNPs in Sn-3Ag-0.5Cu solder improved the spreading and wettability significantly compared to monolithic SAC. It was also revealed that the thickness of the Ag₃Sn IMCs is reduced as compared to the monolithic SAC alloy. Tensile results showed that the composite solder exhibited 13.9 % elongation and 17 % increase in the ultimate tensile strength when 0.05 wt pct GNPs in Sn-3Ag-0.5Cu alloy were added. This was due to the refinement of the IMCs in composite solders compared to the same in Sn-3Ag-0.5Cu alloy brought about by the uniform dispersion of graphene

nanoplatelets [37]. Wang et al. took a similar approach but instead of graphene nanoplatelets they opted for Ni particles to modify the property of Sn_{2.5}Ag_{0.7}Cu_{0.1}RE solder. They found that, results obtained showed that the wettability of Sn_{2.5}Ag_{0.7}Cu_{0.1}RE was largely improved by adding 0.1% Ni in the alloy, and Sn_{2.5}Ag_{0.7}Cu_{0.1}RE_{0.1}Ni exhibited a better wettability than the commercially used Sn_{3.8}Ag_{0.7}Cu alloy [38].

2.3.4 Thermal conduction characteristics

Since most solders are relatively lower melting alloys, it is important that they have relatively good thermal conductivity as to insure not much heat is stored at the solder joint for longevity of solder joints in operation, also solders may also be used in applications such as connecting cooling surfaces as such it is important that they have good thermal contact conductance. Zhang et al. studied the thermal resistance of Sn-Bi solder paste between two Cu plates. A thermal resistance less than 5 mm² K/W was achieved for the Sn-Bi TIM. The Sn-Bi solder also showed a good reliability in terms of thermal resistance after thermal cycling, indicating that it can be a promising candidate for the TIM used for power electronics applications. The experimental data also showed that Sn-Bi solder paste could be a promising adhesive material used to attach power modules especially with a large size on the heat sink [39]. Thermal behaviour is also important during solidification of the solder alloy. During the first stages of solidification the heat transfer from the molten solder to the joint can be represented by a transient heat transfer coefficient. Silva et al. were interested in this transient heat transfer coefficient and wetting angle of Sn–0.7 wt%Cu–(0–0.1 wt%Ni) solder alloys. They found that a decrease in the initial wetting angle means increase in h_i values [40].

2.3.5 Vibration and fatigue behaviour

There are also many application cases where solder joints and materials are subject to vibrations and cyclic loads. Such as automotive electronics industry or controller circuits for heavy duty construction and excavation equipment etc. And for this reason, a look into the vibration absorption and fatigue behaviour is also important for solder materials. Basaran and Chandaroy studied the mechanics of traditional Sn₆₀Pb₄₀ solder alloy under vibrational loads [41]. They found that contrary to popular belief, the solder alloy does not remain in the elastic range regardless of the frequency of loading and the acceleration

level. When the material is in the elastic range, the higher frequency leads to higher damage in each cycle. But when the solder behaviour is inelastic, lower frequency vibrations cause higher damage in each cycle than in higher frequency loads [41]. Song et al. investigated the vibration fracture behaviour of Sn-Bi alloys, with both hypereutectic and eutectic compositors [42]. They found that the damping factor of eutectic composition was grater compared to the hypereutectic samples. The eutectic sample also had grater vibrational fracture resistance as well. Interfriction at eutectic Sn/Bi phase boundaries was regarded as an effective mechanism in absorbing vibration energy [42]. Song et al. likewise investigated the effect of Zn content on vibration behaviour for Sn-Zn and Sn-Zn-Bi alloys [43]. They found that Sn-Zn-Bi alloy (with a Zn content of 5 wt.%) had the poorest damping capacity and the lowest critical vibration cycles to failure due to a hardening effect by Bi and intergranular fracturing. Also, since Zn/Sn interfaces at which internal friction may occur during vibration contribute to the dissipation of vibration energy, Sn-13Zn samples with numerous massive primary Zn needles possess superior damping capacity and vibration life under constant vibration force conditions.

2.4 Electro-Magnetic Properties of Solder Materials

In terms of electrical properties there are only two major ones which have piqued interest of researchers so far; These being the bulk electrical conductivity and electrical conductivity of solder joints. Relevant and notable work regarding these two electrical properties is discussed in the following paragraphs.

2.4.1 Bulk conductivity

In electronic circuits solders are used as interconnects between the PCB and the component which is to be mounted. As a result, the nature of current flow between the circuit board and solder joint is of importance. In this regard Liu and Guo worked in studying the changes in conductivity of tin and Sn-3.0Ag-0.5Cu [44]. They found that after isothermal ageing of the solder joints at 125°C for about 1000hrs, the electrical conductivity of the joints drastically reduced. They attributed this to the formation of microcracks and voids at the solder-PCB interface leading to increased resistance. In SAC solders silver (Ag) is added to improve strength while the presence of copper (Cu) to lower the melting temperature and make the alloy easier to work with [44].

However, these trace additions also have effect on the electrical conductivity of the solders as well. And in this regard, there have also been several investigations into the effects of these trace additions on the conductivity of SAC305 and SAC105 solders. Amin et al. investigated the influence of Ag content had on the electrical conductivity of SAC solders. Their work also dealt with studying the effect of adding trace amounts of iron (Fe) to the said SAC solders [45]. They found that, electrical conductivity increases with increasing the Ag content from 3.0 wt.% to 1.0 wt.%. This they attributed to the increase in the number of low resistivity Ag_3Sn IMCs. Adding Fe to traditional solder also has a similar impact of improving conductivity up till 0.1 wt.% Fe. This decrease in resistivity was attributed to higher conductivity of Fe compared to Sn [45]. Adding Co nanoparticles to SAC387 solders lead to minor change in conductivity while improving mechanical properties noticeably [46]. Çadırlı et al. looked into the electrical and thermal conductivity of directionally solidified Sn–3.5 wt% Ag alloy [47].

Ari et al were more concerned with alloys of zinc and tin. They found that current primarily flows through the pure tin (Sn) phase and as a result the lower the amount of zinc (Zn) in the sample the better its conductivity [48]. They also found that the electrical resistivity has a very strong positive correlation with temperature, that is it increases linearly with temperature with no scatter whatsoever. Thermophysical structure-sensitive properties of Sn-Zn alloys were studied by Plevachuk et al [49]. They investigated two different types of samples, traditional bulk samples and foil samples. They reported that thermal conductivity and electrical conductivity for this alloy followed Wiedemann–Franz–Lorenz law. They also reported that, observing the thermophysical properties of this alloy melts with composition close to eutectic composition revealed the existence of micro zinc phase above the melting temperature [49]. Thermal expansion, electrical resistivity, and spreading area of eutectic Sn-Zn alloys with trace In inclusions were investigated by Gancarz et al. They found that increasing Indium (In) concentration had a negative impact on the conduction property of the tin-zinc system [50]. Same held true for thermal expansion coefficient as well [50]. Gancarz was also involved in another research to modify Sn-Zn alloys with Cu and Ag inclusions for wave soldering [51]. They found that the addition of the inclusions reduced the resistivity and increased the melting temperature of the alloy, however this came at a cost of worsening mechanical properties [51].

With increasing use of photovoltaic cell, solder alloy performance in terms of production of low-cost PV ribbons is also an important issue, with this in mind Chen et al investigated the usage of Sn–0.7Cu–0.2Zn solder alloy with respect to use in PV ribbons. They found that adding trace zinc to the Sn-Cu system improved the resistivity of the solder and Cu interface, due to the reduction in thickness of the intermetallic layer [52]. Kumar, Behera and Mohan tried to create Indium (In) based Sn-Bi-In alloy systems. They found that the increase in In content leads to a reduction in the electrical conductivity [53].

Sn-Al systems are a great candidate for high temperature solder as they have excellent conductivity, strength and high temperature sustainability. Infact for these reasons they are a viable candidate for high power transmission [54], though research into them as potential solder alloys is rare at the best. With that said one of the recent works in to Sn-Al systems were done by Tezel et al [55]. Their investigations revealed that in general for any composition of Al, the electrical resistivity is lower than that of pure Sn [55].

Guo and others investigated the electric conduction behaviour of bulk Sn-Ag alloys and joints in comparison to pure tin under thermal aging and shock [56]. They found that aging at 150 °C, both the Sn-Ag alloy and pure Sn show similar reduction in conductivity, while the Cu solder joints experience a significant drop in conductivity [56]. Sn and Sn-Ag also show similar decrease in conductivity under similar thermal fatigue cycles as well [56].

2.4.2 Solder joint conductivity

One of the earlier and more notable investigations into the properties of lead-free solder joints was conducted by Kang et al. Though in this section only talks about their studies into the electrical resistivity of solder joints, they also evaluated the mechanical properties as well. For the substrate they used Cu and Ni(P)/Au. They found that the presence of intermetallic compounds increased the resistance of solder joints as it did for bulk alloy samples [57]. Cook et al. studied the solder joint resistivity of Sn-Ag, Sn-Ag-Cu, and Sn-Ag-Cu-X alloys (where X is Co, Fe, or Bi). The resistivity in all joints initially increased with temperature and reached a constant steady-state value with time [58]. Since solders are used for joining a myriad of different materials in different applications, the effect of substrate material on the solder joint along with the alloy used itself has a significant effect on the conduction characteristics of the joint. Also, different soldering methods can

also have an impact on the solder joint property. In that light most recent investigations have focused on different types of substrate and alloy combinations. Sonawane et al. compared the solder joint performance of SAC/Cu solder joints soldered using two different soldering techniques (Concentrated Solar Energy Soldering and Conventional Soldering Iron). They found that the CSE joints had better conductivity compared to conventional soldering techniques [59]. Cheng et al. studied the solder joint characteristics of a common thermoelectric material, Bi_2Te_3 . They found that Ni electrodeposit improved the conductivity of the solder-material interface [60]. Though inclusion of carbon nanotubes improves the mechanical properties of SAC solders, the effect on its joint conduction characteristics is not so simple. In that light Ismail et al. investigated solder joints of SAC305 with carbon nano tube inclusions. They found that electrical resistivity of Sn–3.0Ag–0.5Cu solder joint increased with the incorporation carbon nanotube up to 0.03 wt% and slightly decrease at 0.04 wt% [61]. One of the more interesting applications of solder alloys is in the joining of coated conductor high temperature superconducting tapes. Drienovsky et al. investigated the nature of such joints in their work. As soldering material, they used near eutectic and hypoeutectic SAC alloys. They observed that soldered joints with near eutectic solder alloy (SAC305) exhibited the smallest joint resistivity [62].

Now that some of the recent and relevant works in the development of lead-free solder alloys have been presented, as stated earlier, not one of them has focused on the AC magnetic or the dielectric properties. These two properties are quite important in circuitry and equipment subjected to electromagnetic signals such as network equipment. Neither has any work tried to compare and contract these various different alloy systems in terms their mechanical, bulk conduction, AC dielectric and Magnetic properties. And it is this gap that the present work hopes to fill.

CHAPTER-3

MATERIALS AND EXPERIMENTAL DETAILS

3.1 Materials for Test Material Preparation

The materials used for the current study are lead (Pb), tin (Sn), zinc (Zn), bismuth (Bi) and aluminium (Al). Before Perpetration of the samples, the purity of the samples was determined through X-Ray Florence Radioscopy (XRF) at the Multi Scale Characterization Laboratory. It was observed that all the ingots selected were sufficiently pure and suited for the preparation of the samples. The composition of the elements is given in the table below.

Table 3. 1 Chemical composition of the raw ingots used

Ingot Name	Composition (%)						
	Sn	Pb	P	Zn	Bi	Al	Fe
Tin (Sn)	99.13	-	0.87	-	-	-	-
Lead (Pb)	-	99.84	0.18	0.98	-	-	-
Zinc (Zn)	-	-	-	99.58	-	-	0.42
Bismuth (Bi)	-	-	0.22	-	99.78	-	-
Aluminium (Al)	-	-	0.5	-	-	99.5	-

3.2 Test Material and Reference Solder Material Preparation

Four main alloy systems were chosen for this work. Those are the conventional Sn-Pb alloy system, Sn-Bi alloy system, Sn-Zn alloy system and Sn-Al alloy system. For the comparison among the traditional lead-tin and replacement systems a suitable fixed composition was chosen. This composition was 80% tin with the remaining 20% one of the four other elements. Also trace amounts of copper at 0.1, 0.3 and 0.5% were added to the Sn-(Zn/Bi/Al) systems to study the effects on their properties. A separate Sn50Pb50 alloy was also made to study the effects of lead in traditional Sn-Pb systems to see if lowering amount of lead has any significant downsides in terms of mechanical and

electrical properties. For preparation of the samples, first the elements were melted inside an electric furnace, the mixture was periodically checked and stirred to ensure proper distribution of the elements, then after the complete melting of the elements the samples for electric and mechanical testing were die casted. Additional samples of Sn63Pb37 and Sn96.5Ag3Cu0.5 (SAC305) were also made as reference alloys for comparative analysis.

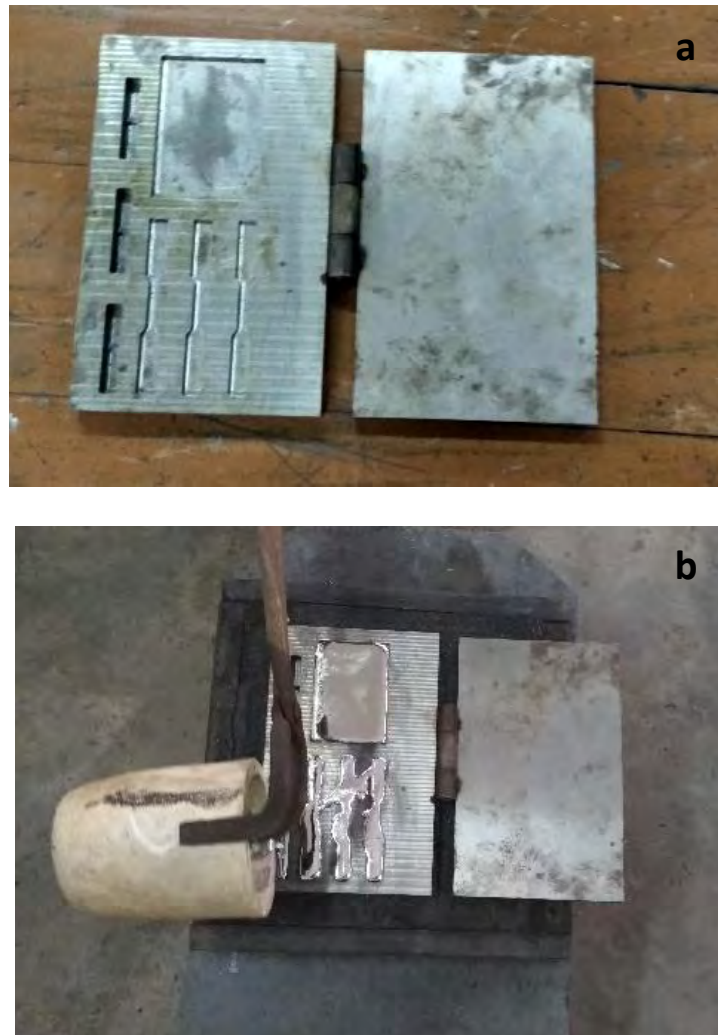


Figure 3. 1 Photographs of (a) Casting die, (b) Preparation of the samples

The specimens were finally left to cool under natural conditions. After solidification samples for the mechanical and electrical investigations were fabricated. For mechanical characterization samples for impact, hardness and tensile strength were fabricated. For ac and dc characterization tetragonal samples were made.

3.3 X-ray Fluorescence (XRF) Analysis

After preparation of the test alloys as well as the reference alloys, X-ray fluorescence analysis was carried out to check if the samples had the desired composition. The analysis was carried out using Shimadzu XRF-1800 at the Multi Scale Characterization Laboratory. The chemical compositions of both the experimental and reference alloys given in the following tables.

Table 3. 2 Chemical composition of the binary and ternary alloys developed

Serial no.	Alloy samples	Nominal Compositions (wt%)	XRF Chemical Compositions (wt%)					
			Sn	Bi/Zn/Al	Mg	Si	Fe	Cu
1	Sn20Bi	80% Sn-20% Bi	79.910	19.70	0.13	0.15	0.11	-
2	Sn19.99Bi0.1Cu	79.91% Sn-19.99% Bi-0.1% Cu	Bal.	19.95	-	0.01	0.02	0.15
3	Sn19.94Bi0.3Cu	79.76% Sn-19.94% Bi-0.3% Cu	Bal.	19.91	-	0.03	0.01	0.29
4	Sn19.9Bi0.5Cu	79.6% Sn-19.90% Bi-0.5% Cu	Bal.	19.88	-	0.02	0.03	0.52
5	Sn20Zn	80%Sn-20% Zn	79.788	19.852	0.09	0.27	-	-
6	Sn19.99Zn0.1Cu	79.91% Sn-19.99% Zn-0.1% Cu	Bal.	19.912	0.035	-	0.021	0.099
7	Sn19.94Zn0.3Cu	79.76% Sn-19.94% Zn-0.3% Cu	Bal.	19.89	0.054	0.01	0.03	0.33
8	Sn19.9Zn0.5Cu	79.6% Sn-19.90% Zn-0.5% Cu	Bal.	19.87	0.03	-	0.05	0.48
9	Sn20Al	80% Sn-20% Al	79.828	19.801	0.170	0.134	0.060	-
10	Sn19.99Al0.1Cu	79.91% Sn-19.99% Al-0.1% Cu	Bal.	19.971	0.021	0.038	-	0.17
11	Sn19.94Al0.3Cu	79.76% Sn-19.94% Al-0.3% Cu	Bal.	19.895	0.041	-	0.061	0.320
12	Sn19.9Al0.5Cu	79.6% Sn-19.90% Al-0.5% Cu	Bal.	19.863	0.075	0.024	0.034	0.510

Table 3. 3 Chemical composition of the reference solder materials

Serial no.	Alloy samples	Nominal Compositions (wt%)	Measured Chemical Compositions (wt%)					
			Sn	Pb	Ag	Cu	Si	P
1	Sn63Pb37	63% Sn-37% Pb	63.85	36.09	-	-	0.02	0.06
2	Sn96.5Ag3Cu 0.5	96.5% Sn-3% Ag- 0.5% Cu	96.77	0.07	2.82	0.34	0.02	-

Some other elements are present in all the alloy samples. In most cases the amount of these other elements is less than 0.1 % which should be reasonably low as to not impact the properties of the alloys. The crucible was always cleaned before casting of each alloy. The most probable cause for these elements would be the furnace walls. Also, the casting of the alloys was done under normal ambient conditions so another cause of these elements may be the environment. A third probable cause could be the graphite powder that was used on the casting die. Impurities mixed with this this graphite powder may have infiltrated during cooling of the alloys.

3.4 Preparation of Mechanical and Electrical Test Specimens

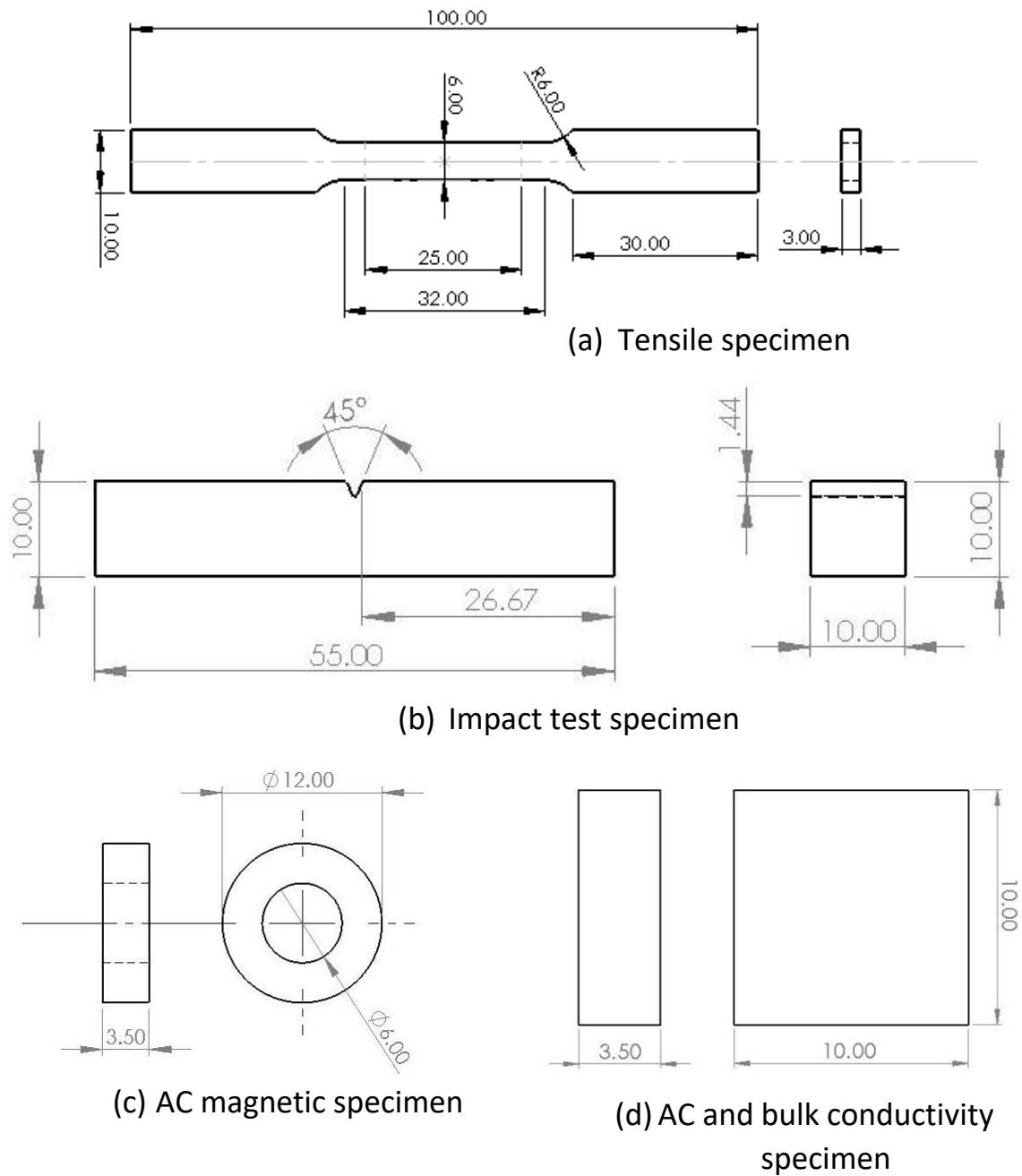
For each test alloy system, two impact and two tensile test specimens were fabricated. Along with these two additional samples for microstructure analysis and electrical investigations were also made. The tensile samples were first die casted as seen in figure 3.1 (b) then polished using emery paper to removes excess material from the corners and edges. All the tensile specimens were fabricated according to ASTM standards (E8/E8M). The specimens for the Charpy test were also made according to ASTM standards.

The tensile samples have a gauge length of 25mm, width of 6mm a thickness of 3mm and a fillet radius of 3 mm. The Charpy impact test specimens were 55mm in length 10 mm in width and height with a 45° V-notch 0.25 mm radius along the base (ASTM E23). Samples prepared for microstructure and hardness tests were 18mm×18mm×4mm in dimensions. Special samples of smaller dimensions (10mm×10mm×3.5mm) were prepared for AC measurements. After fabrication of the electric and microstructure specimens, they were progressively polish with finer grade emery paper until mirror finish was obtained. The grades of emery paper used were, 120, 320, 600, 800 and 1200.

In the following tables the dimensions for the tensile strength and the parameters for the Charpy test are given.

Table 3. 4 Dimensions of tensile test specimen

Symbol	Description	Dimension (mm)
G	Gauge length	25
A	Length of reduced parallel section	32
L	Overall length	100
W	Width	6
R	Radius of fillet	6
T	Thickness	3
B	Length of grip section	30



Dimensions in millimetres (mm)

Figure 3. 2 Schematic illustrations of Mechanical and Electrical test specimens with major dimensions: (a) Tensile specimen, (b) Impact Test specimen, (c) AC and Bulk conductivity specimen and (d) AC Magnetic specimen



Figure 3. 3 Actual photographs of mechanical, electrical and magnetic test samples

3.5 Mechanical Characterizations

3.5.1 Tensile test

Tensile characteristics were carried out using a double column universal test frame with a maximum load capacity of 10 kN (Shimadzu tensile tester, AGS-X series) over at the Solid Mechanics Laboratory, Department of Mechanical Engineering, BUET. The machine was linked to a computer and the data for force exerted and displacement of the specimen was recorded in real time. 3 samples for each of the alloys and their individual constituents were tested till failure in this manner. After each test the data was for force vs displacement was exported onto a separate recordable media in .CSV format and later used to plot the stress vs. strain plots as well as to determine the ultimate tensile strength and maximum elongation.

Strain rate is an important parameter in tensile testing. In this regard, a suitable strain rate needs to be chosen. In this experiment the extension/cross-head speed was held constant at 1.5 mm/min. The relation between conventional strain rate and extension/crosshead velocity is,

$$\frac{de}{dt} = \frac{d(L-L_0)/L_0}{dt} = \frac{v}{L_0} \dots \dots \dots (3.1)$$

Where v is the extension/crosshead speed and L_0 is the gauge length. So, the strain rate come out to be 0.001/s. which is reasonably low to express both the elastic and plastic characteristics of the specimens properly.

The force displacement/extension data found from the universal testing machine was converted to engineering stress and strain plots by dividing the force values (P) with the

cross-section of the gauge which was measured using a slide calliper. To account for the variation in the area of the gauge, total 10 readings of width(w) and thickness(t) from different sections were taken and averaged to get the final area (A). The displacement/extension(x) was converted to engineering strain by normalizing by the gauge length (L_0).

$$\sigma = \frac{P}{A} ; \varepsilon = \frac{x}{L_0} \dots\dots\dots (3.2)$$



Figure 3. 4 Tensile tester

3.5.2 Charpy impact test

Impact characteristics are also another important consideration for solder interconnects. Impact means the sudden application of high load for a short duration of time. In this specific context impact resistance of a material means its ability to sustain sudden high loads even with the presence of small fractures and defects. The higher the impact resistance the better the solder material for use in regular operations. To characterize the materials in this regard, Charpy impact test or Charpy notch toughness was used. The greater the energy absorbed in Charpy notch toughness test, the better suited the alloy for use as electronic interconnects.

Charpy impact test involves the determination of energy absorbed by a material with a V or U notch. In this investigation a 45 V-notch with 2mm depth was chosen. Before testing of the experimental alloys, the apparatus was swung without any test specimens. The

angle of this run (α) was recorded. This is because there is some energy loss due to friction which needs to be accounted for in the calculation. After that the test specimens were placed in on the platform in the orientation needed for Charpy test and angle at the end of swing (β) was recorded. Then using the arm length(R), mass of hammer (m) and gravitational acceleration (g) the energy absorbed by the specimens were recorded. For each specimen total two samples were tested and the average of the two readings were taken as final. The values of the individual runs were also compared to each other in order to see if any internal defects were present inside the specimen. The Charpy tests parameters are given in the table below along with the formulation to calculate the impact energy.

$$E = mgR.(\cos \beta - \cos \alpha) \dots\dots\dots (3.3)$$

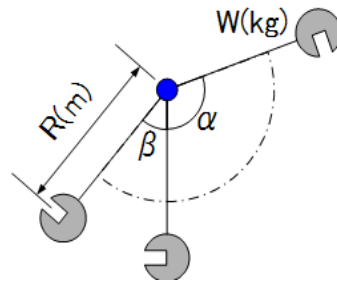


Figure 3. 5 Charpy Impact Test Angles.



Figure 3. 6 Charpy impact tester

Table 3. 5 Charpy Test Parameters and Their Standard Values

Parameter	Value
Angle of fall, α	139.5°
Angle at the end of swing, β	As recorded at the end of each run
Arm length, R	0.825 m
Mass of the hammer, m	20.24 kg
Gravitational acceleration, g	9.81 m/s ²

3.5.3 Vickers hardness test

The microhardness of the alloys was measured using a microhardness tester. Three measurements were done for each of the alloys. The force applied by the indenter was 50 gm and the dwell time was 10s. The angle between the opposite faces of the diamond indenter was 136°. The average of the three measurements were taken for the final microhardness value. The hardness was calculated using the equation,

$$HV = \frac{2F(\sin\frac{136}{2})}{d^2} \dots\dots\dots (3.4)$$

Where, F = the applied force by the indenter (in Kgf)

d = Mean diagonal of indentation (in mm)

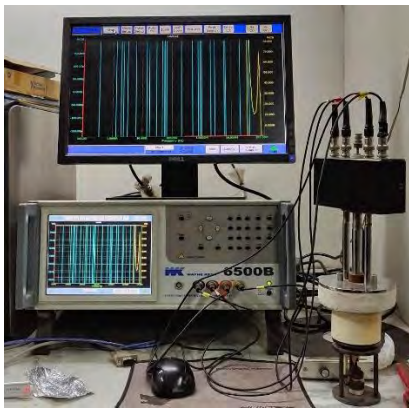


Figure 3. 7 Microhardness tester

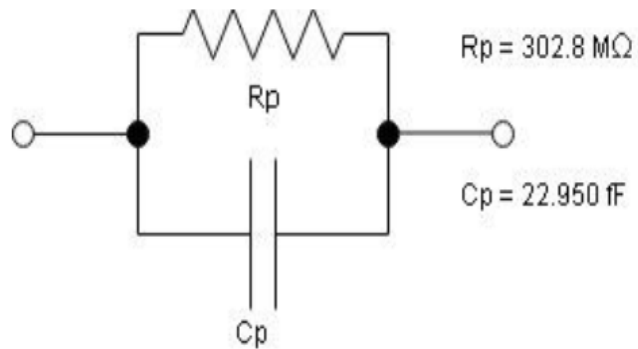
3.6 Electro-Magnetic Characterizations

3.6.1 Complex dielectric constant and loss tangent test

The dielectric characteristics of the materials at various frequencies were investigated using an impedance analyser (WK 6500B) over at the Material Science Laboratory-II, department of Physics. The materials were modelled as parallel equivalent circuits with a purely resistive element and a purely capacitive element in parallel for the dielectric investigations. While for the impedance characteristics modelled as series equivalent circuit with a purely resistive element and a purely capacitive element in series. For finding the correct models for the materials, both automatic circuit from the analyser as well as manually entering the values of the resistive and capacitive elements were looked into. A typical equivalent model for the dielectric characterization of a sample is shown below along with the image of the analyser itself.



(a)



(b)

Figure 3. 8 (a) Impedance analyser (b) Equivalent circuit model for dielectric characteristics

The data obtained from the impedance analyser included the capacitance C of the material at different frequencies as previously mentioned. The dielectric constant then needs to be found from this capacitance information by means of the physical dimensions of the sample, area (A) perpendicular to the connection and the thickness (d) along the applied voltage direction. The data for the loss tangent ($\tan \delta$) is directly recorded by the machine.

$$\epsilon = \frac{Cd}{A} ; \epsilon_r = \frac{\epsilon}{\epsilon_0} \dots\dots\dots (3.5)$$

3.6.2 AC magnetic permeability test

The complex permeability of the samples was also measured using the impedance analyser as well. In order to do so the toroid shaped samples were first wound with insulated copper wire. And then connected to the analyser. In this case, each of the samples were modelled as an ideal inductor, in series with an ideal resistor. Real and imaginary parts of permeability were found from L_s/L_0 and $R_s/L_0\omega$. Here, L and L_0 are the inductance of solenoid with and without sample, R_s is the AC resistance of the specimen and ω the frequency of the applied field. The calculation was done automatically by the analyser. The average flux path length (l_e), the number of turns (N) and the toroid cross section (A_e) were entered.

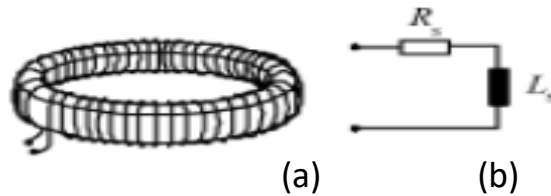


Figure 3. 9 (a) Wound toroid sample, (b) equivalent circuit [63].

The values for the L_s and R_s are directly measured by the analyser. The equations used by the impedance analyser for the purpose of finding the complex relative permeability are:

$$\mu' = L_s \left(\frac{l_e}{\mu_0 N^2 A_e} \right) \quad \mu'' = R_s \left(\frac{l_e}{\omega \mu_0 N^2 A_e} \right) \dots\dots\dots (3.6)$$

3.6.3 Bulk conductivity test

For measurement of bulk conductivity, the resistance of the specimens was first measured using a micro-ohm meter. Then the dimensions of sample, the cross-section area normal to the applied voltage (A_f) and the length in the direction of the voltage (d) were measured. These dimensions were then used to find out the conductivity of the material. The measurements were carried out at High Voltage Engineering Laboratory, department of Electrical and Electronic Engineering.

$$\sigma = \frac{1}{R} \left(\frac{d}{A_f} \right) \dots\dots\dots (3.7)$$



Figure 3. 10 Micro-ohmmeter

3.7 Optical Microscopic Observation

Photo micrographs of the test alloys as well as the constituent elements were taken using a Nikon Eclipse LV150 microscope over at the metallography laboratory, department of Materials and Metallurgical Engineering. The relationship between the different mechanical, electrical and magnetic properties and microstructure of the different materials were explored. The magnification level chosen was 500X, the highest possible by the instrument.



Figure 3. 11 Optical microscope

3.8 Scanning Electron Microscope Observation

SEM imaging and EDS analysis of the alloy samples and constituent materials were also performed to better understand the surface composition and microstructure. The equipment used was JEOL JSM 7600F manufactured in Japan. EDS analysis was done by JED-2300 Analysis Station also manufactured in Japan.



Figure 3. 12 Scanning electron microscope

CHAPTER-4

MICROSTRUCTURAL OBSERVATIONS

4.1 Optical Microscopic Observations

Figures 4.1, 4.2, 4.3 and 4.4 show the microstructure of the constituents and alloys at various percentage of copper. As mentioned before with the increase in copper, various intermetallic phases are seen developing in the micrographs for all of the alloys. In the case of bismuth system, it can be seen that there are two distinct phases, one being the solid solution of β -Sn and Bi, the other being the concentrated lumps of bismuth [64]. As copper is introduced, it can be seen that it removes β -Sn both from the base alloy starts to form intermetallic compounds between itself and tin [65]. For the aluminum system, before doping by copper there are two distinct regions present just like that of the bismuth system. These are the eutectic phase and the dendritic aluminum rich phase as aluminum does not dissolve with tin in solid state [66]. Once again with the inclusion of copper intermetallic phases are formed aluminum resulting in the substituent reduction of these dendritic aluminum phases as can be seen in the micrographs. For zinc alloys, initially there are once again two distinct regions present, the alternating laminates of zinc and tin in the eutectic region and the long slender needle like zinc crystals as zinc is also not soluble in tin at solid state. For this alloy system it can be noticed that with increased amounts of copper the presence of the zinc needles is gradually reduced and the eutectic structure is refined along with the formation of intermetallics [67]. The presence of these intermetallic compounds is what leads to the increased strength, hardness and lowered elongation and impact for all the alloys.

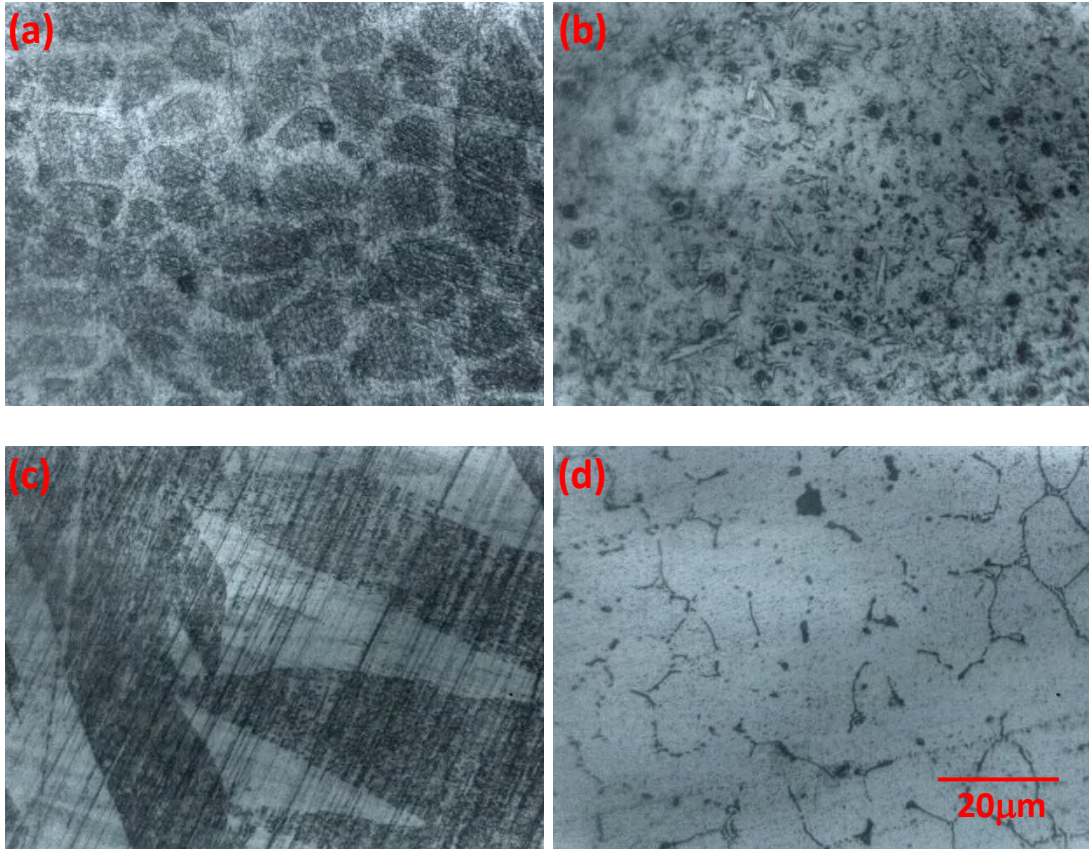


Figure 4. 1 Micrographs of constituent elements: (a) Sn, (b) Zn, (c)Bi and (d) Al

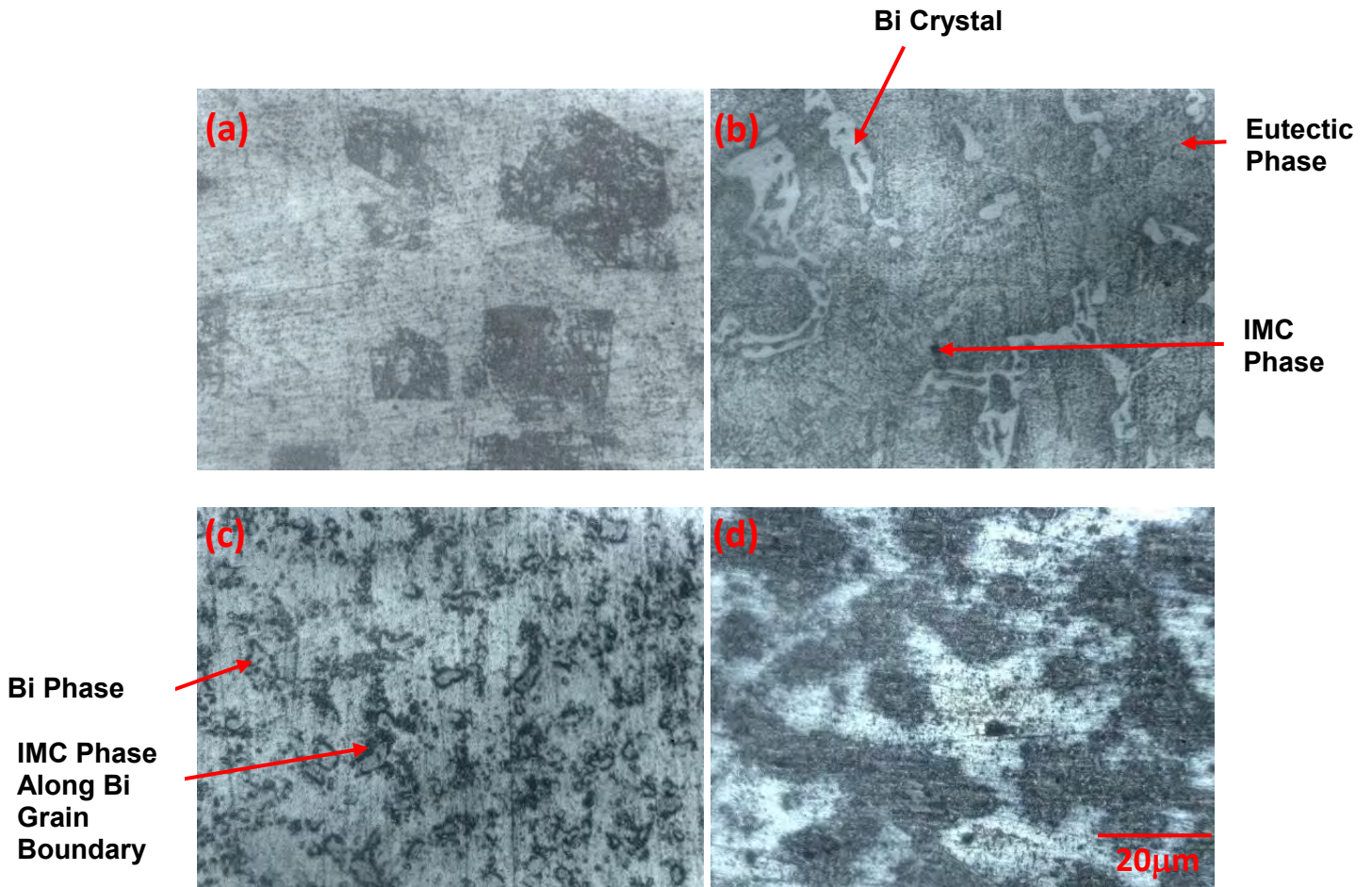


Figure 4. 2 Photomicrographs of Sn-Bi material system with trace addition of Cu: (a) Sn-20wt%Bi, (b) Sn-19.9wt%Bi-0.1%Cu, (c) Sn-19.7wt%Bi-0.3%Cu, (d) Sn-19.5wt%Bi-0.5%Cu

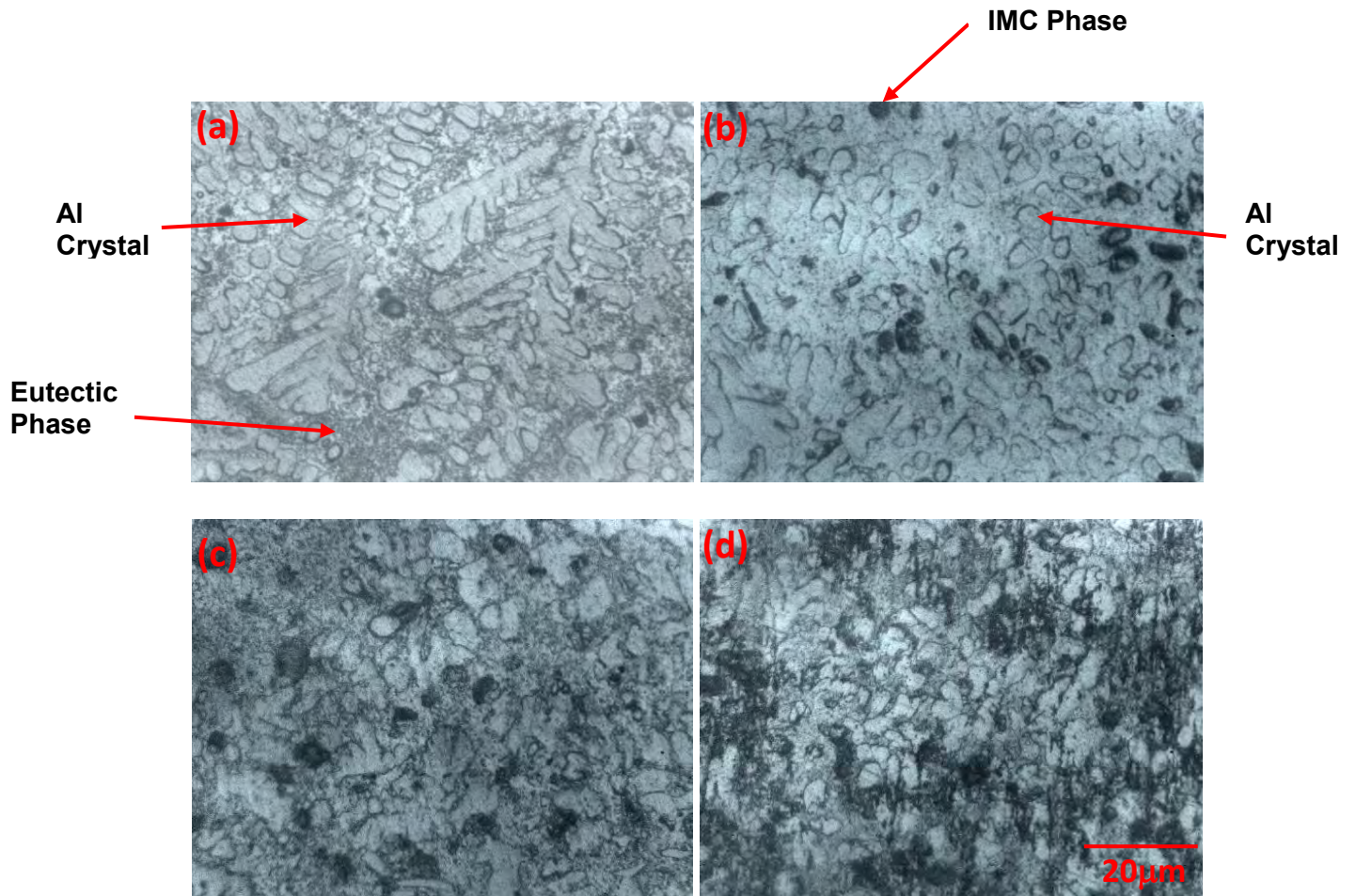


Figure 4. 3 Photomicrographs of Sn-Al material system with trace addition of Cu: (a) Sn-20wt%Al (b) Sn-19.9wt%Al-0.1%Cu, (c) Sn-19.7wt%Al-0.3%Cu (d) Sn-19.5wt%Al-0.5%Cu

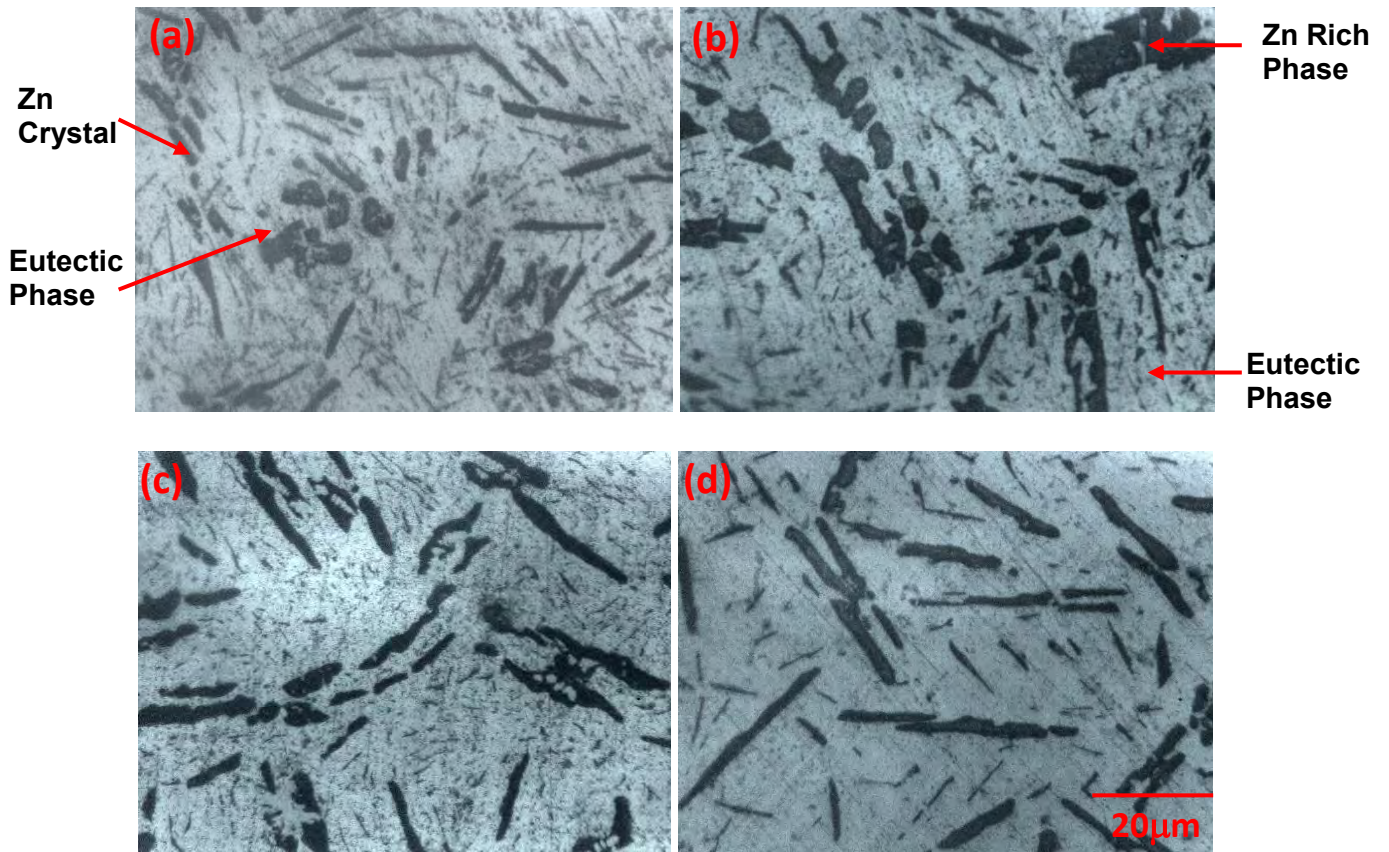


Figure 4. 4 Photomicrographs of Sn-Zn material system with trace addition of Cu: (a) Sn-20wt%Zn (b) Sn-19.9wt%Zn-0.1%Cu, (c) Sn-19.7wt%Zn-0.3%Cu (d) Sn-19.5wt%Zn-0.5%Cu

4.2 SEM and EDS analysis

Figures 4.5-4.10 shows the SEM images at 1000x magnification and EDS spectrum of the specimen surfaces. EDS analysis mainly helps in identifying the phase distribution inside a sample. Though the image is of a single layer of a specimen but, by observing this said layer and noting the different areas of the different phases an idea about the phase distribution through the whole sample can be gained. Two such reports for each specimen are presented. One showing the SEM and EDS analysis of the entire layer, the other showing the analysis of noticeable features. Taking a look at the reports for the analysis done at entire layer of the specimens shows that, there is a difference in the chemical composition from the ones performed earlier. This analysis is performed only at the thin surface level of the material, meaning it only shows the different constituents at that specific layer. The discrepancy between the EDS reports and earlier chemical composition indicates that the different phases are not distributed uniformly throughout the entirety of the sample. Which is to be expected as the alloys were made to from under normal ambient conditions. No specific drawing, annealing or other heat treatment method was used to give the alloys a more uniform and homogeneous microstructure throughout. A consequence of this phenomenon maybe why the dielectric function and loss plots show slight deviations from the expected curves. In figures 4.6 and 4.8 there can be seen distinct circular white spots which are rich in copper. In both these cases at these spots the with the presence of copper there is also the presence of tin (figure s 4.6,4.8) and aluminium (figure 4.8). This indicates that with the introduction of copper, intermetallic compounds are formed between itself and other alloy constituents. In the case of the 0.5% copper doped sample of aluminium specially, the white spots are closely located to the aluminium dendrites and the EDS report suggests the presence of two intermetallic compounds, one between copper and tin and the other between aluminium and tin. The report also indicates that the formation of intermetallic compounds between tin and copper is grater compared to that of the compounds between aluminium and tin. Also, the formations of these IMC indicate that, copper atoms help to eject Sn and Al from the bismuth and aluminum increasing the eutectic composition in alloys. Also, for the zinc system in figure 10 indicates that the copper particles have primarily been absorbed in the zinc rich needle like phase helping to reduce the needle like formations. There can also be seen a white phase along the zinc grains which indicates intermetallic compound formation between Zn and Cu.

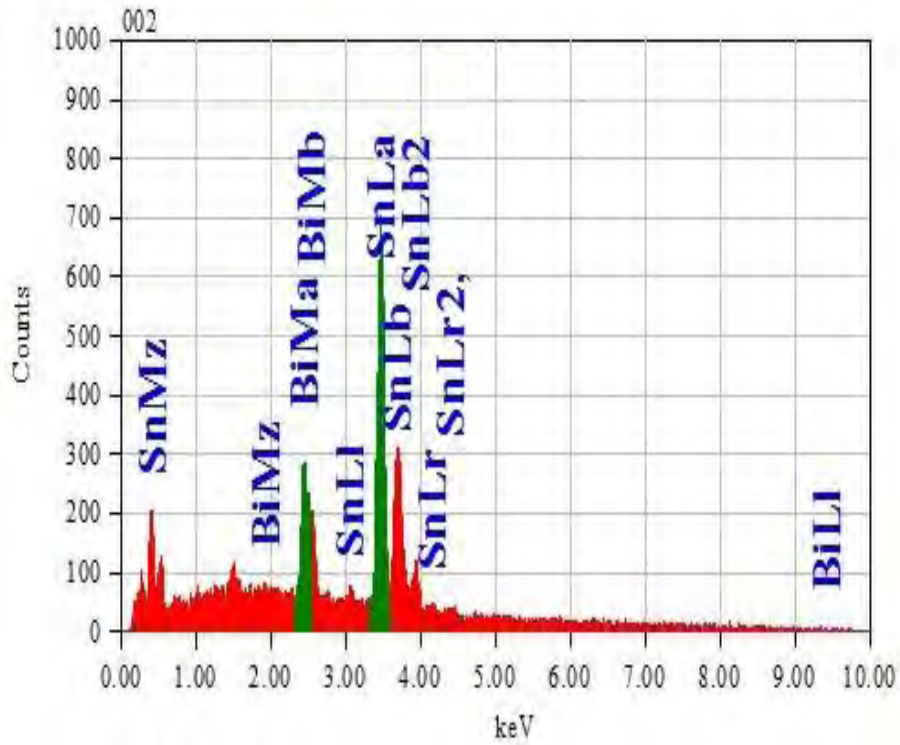
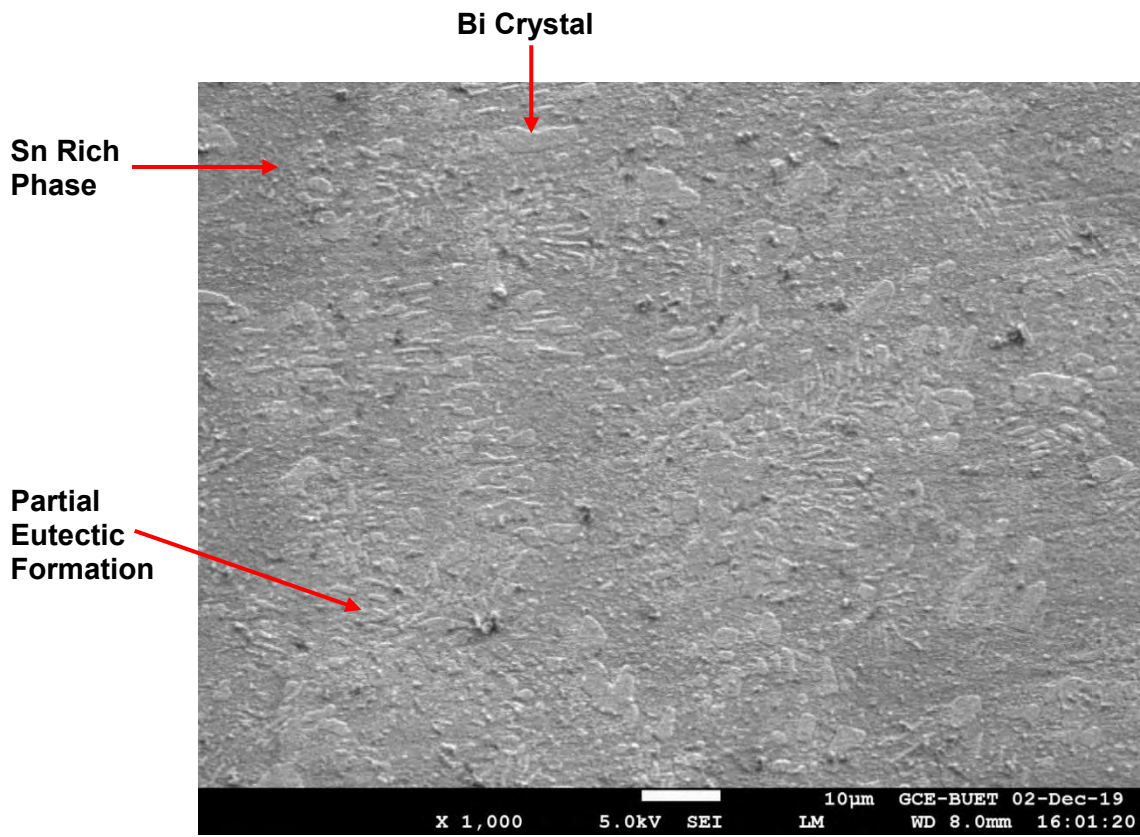


Figure 4. 5 SEM image and EDS analysis of Sn₂₀Bi sample

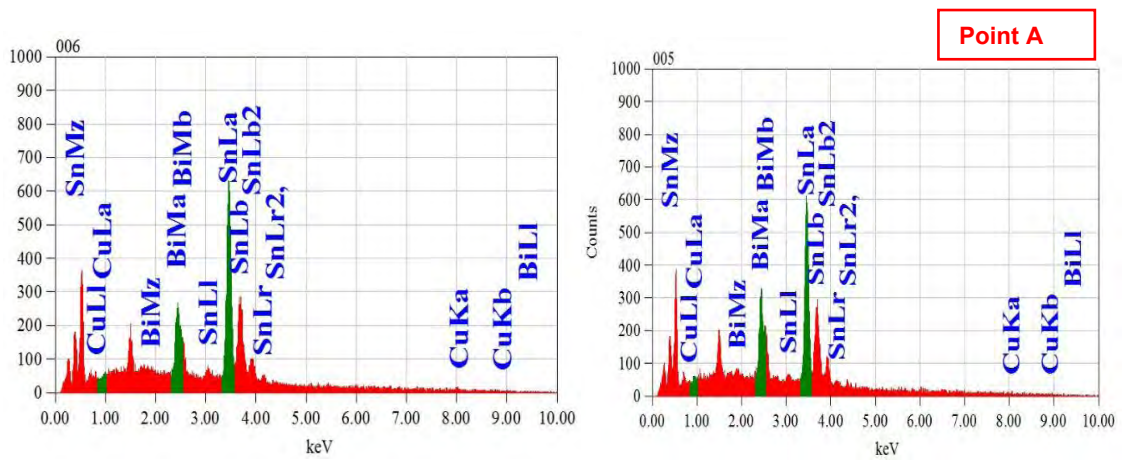
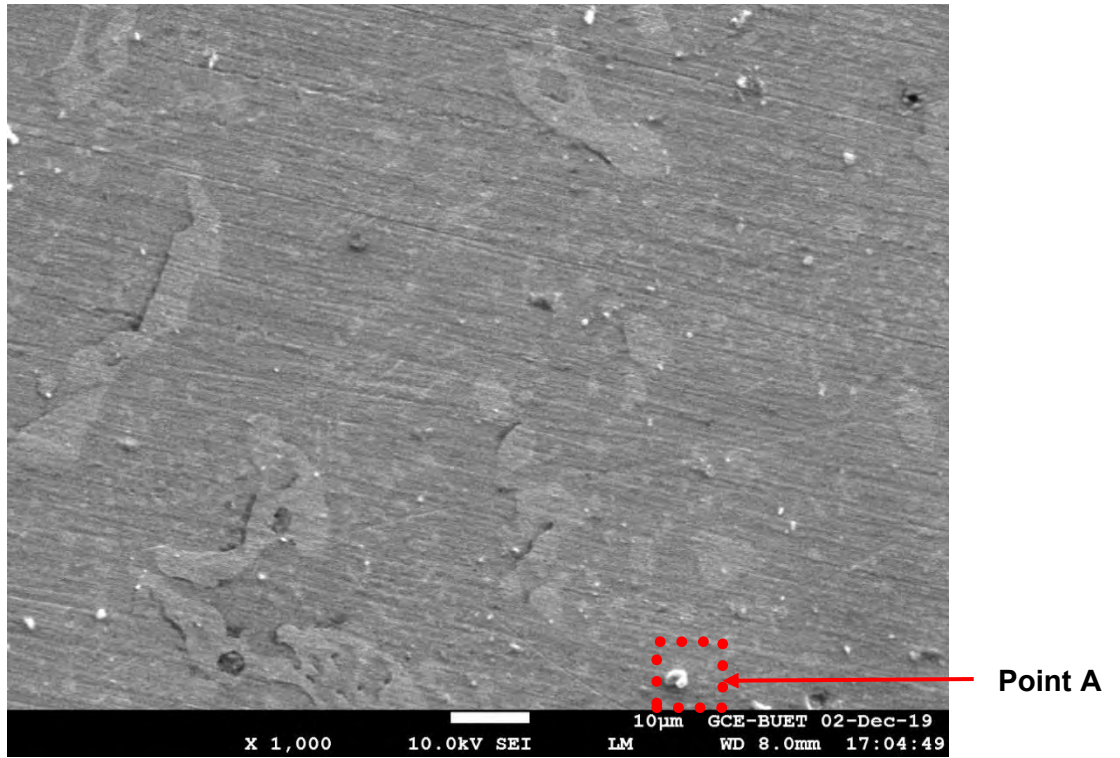


Figure 4. 6 SEM image and EDS analysis of Sn19.90Bi0.5Cu sample

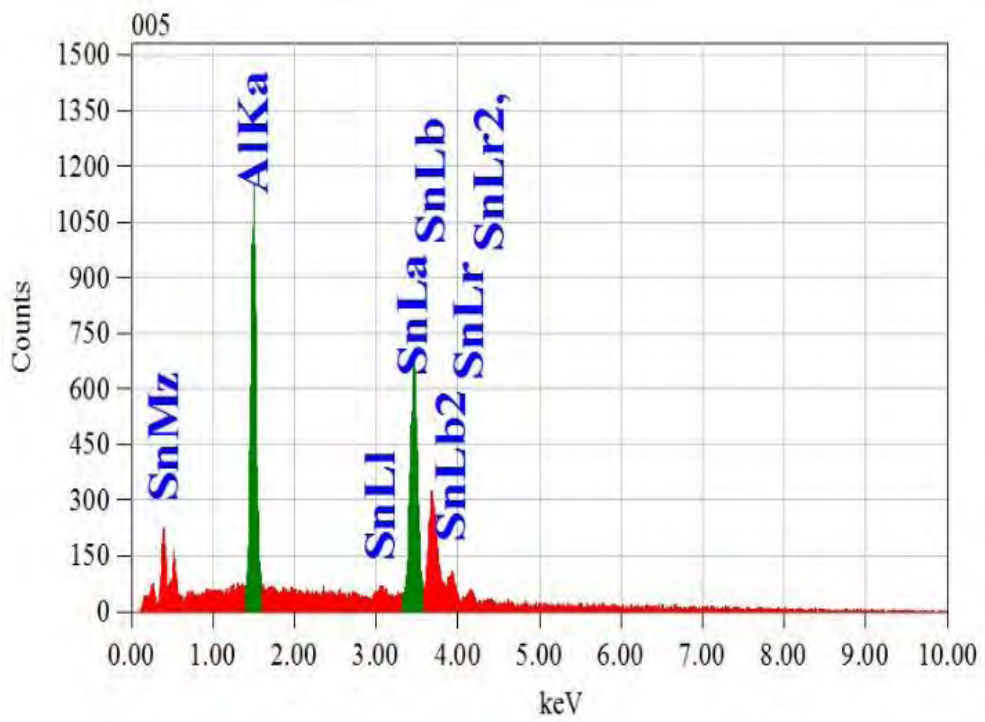
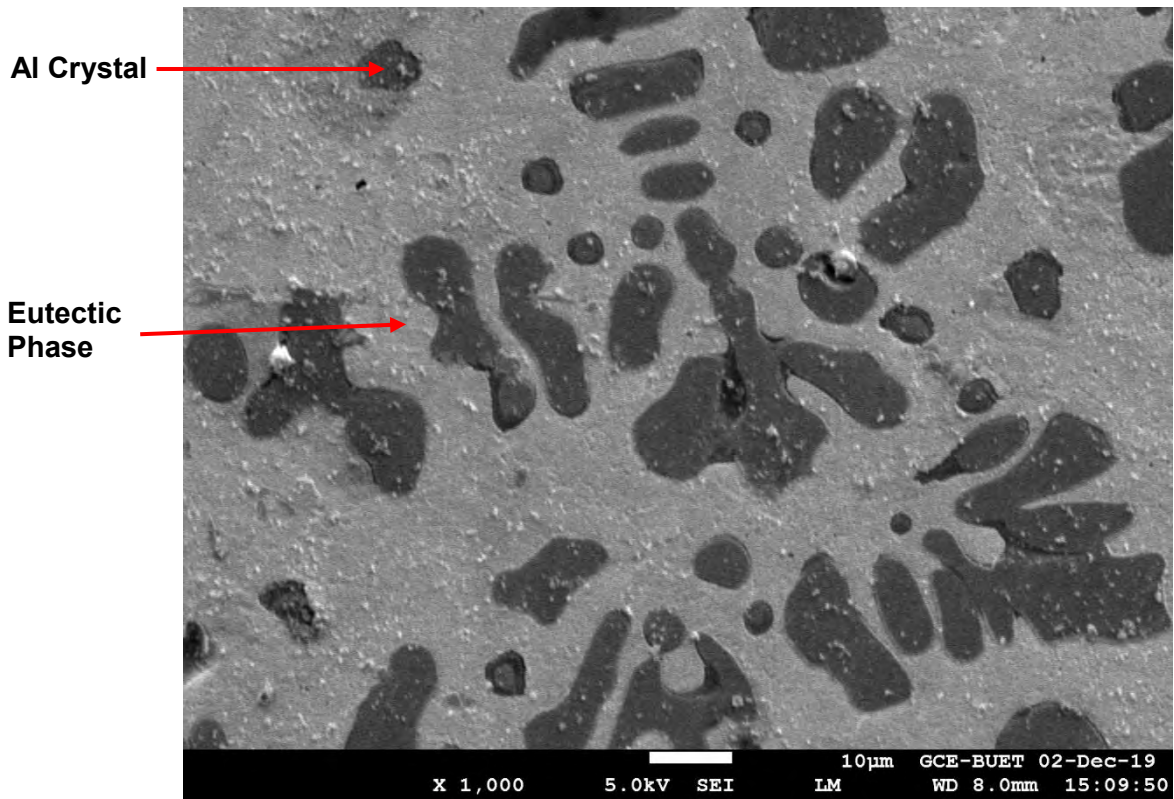


Figure 4. 7 SEM image and EDS analysis of Sn20Al sample

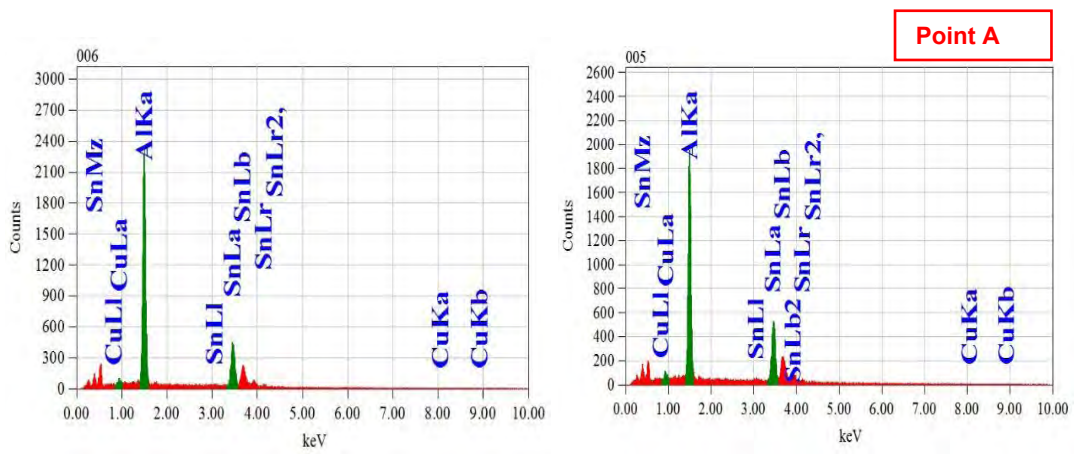
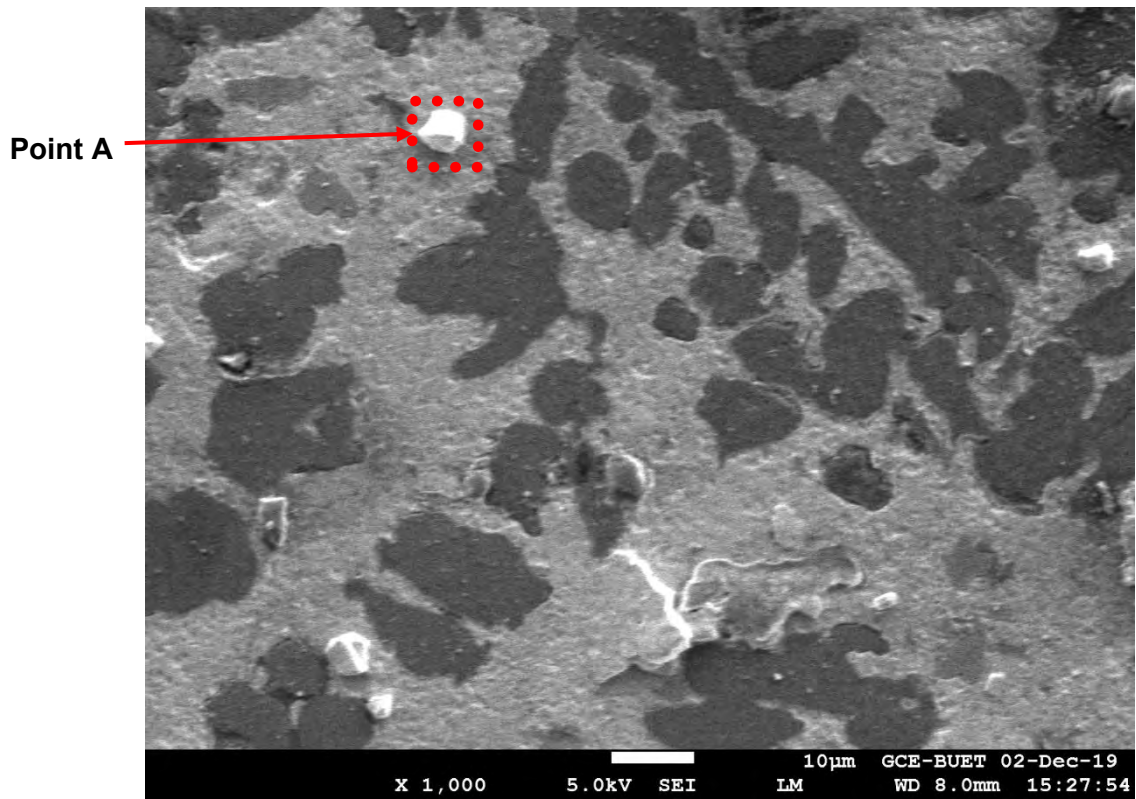


Figure 4. 8 SEM image and EDS analysis of Sn19.90Al10.5Cu sample

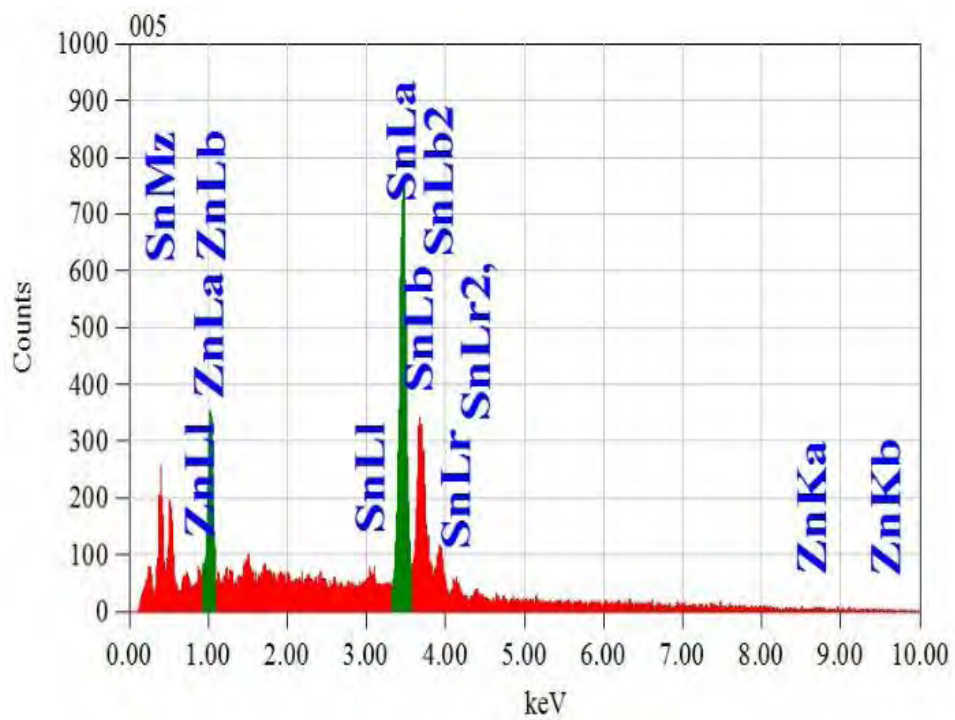
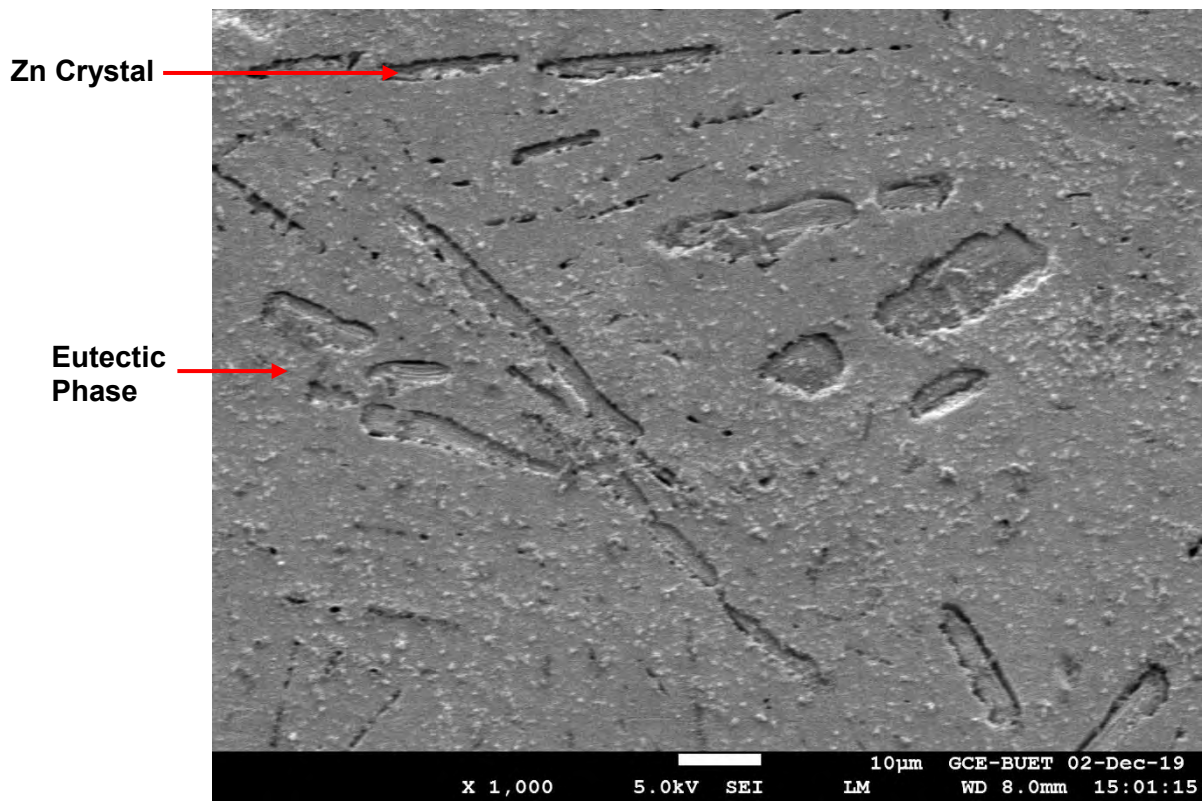


Figure 4. 9 SEM image and EDS analysis of Sn₂₀Zn sample

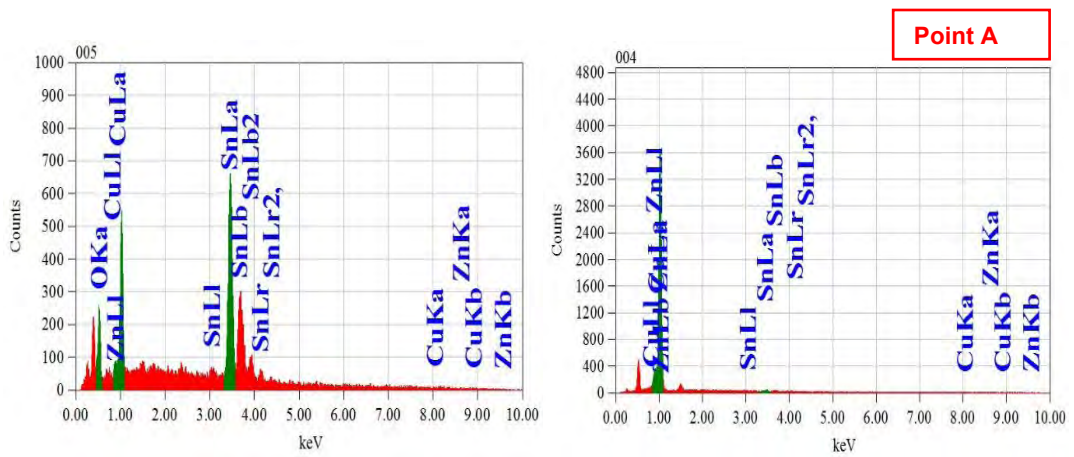
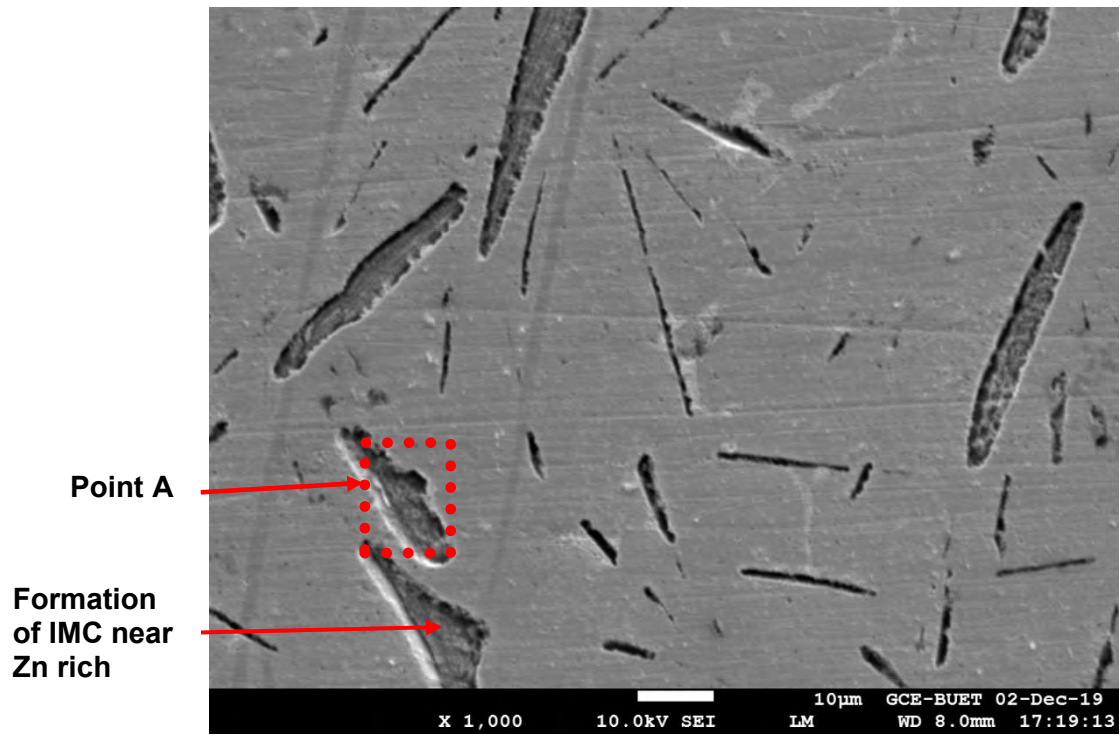


Figure 4. 10 SEM image and EDS analysis of Sn19.90Zn0.5Cu sample

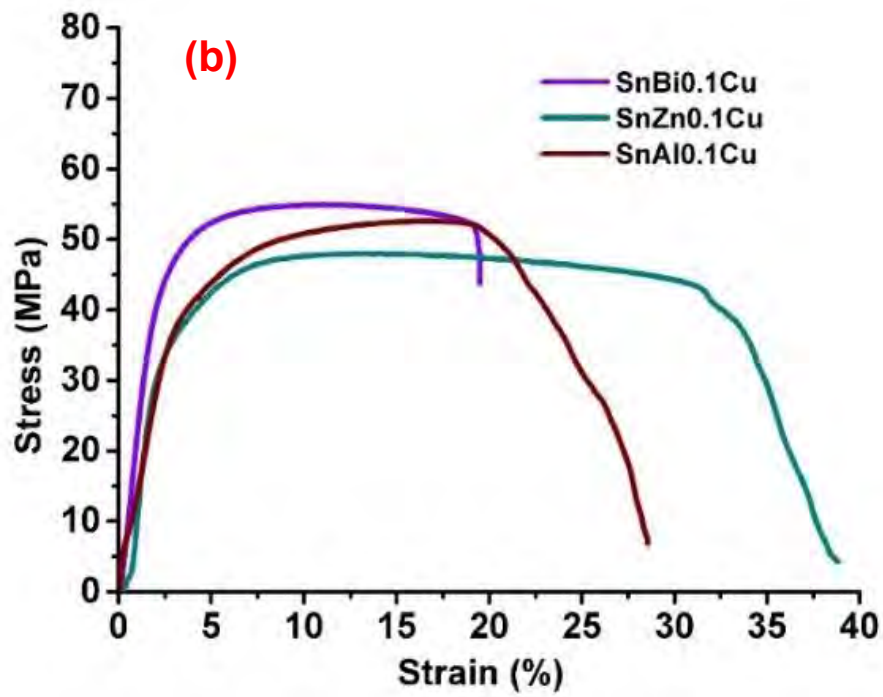
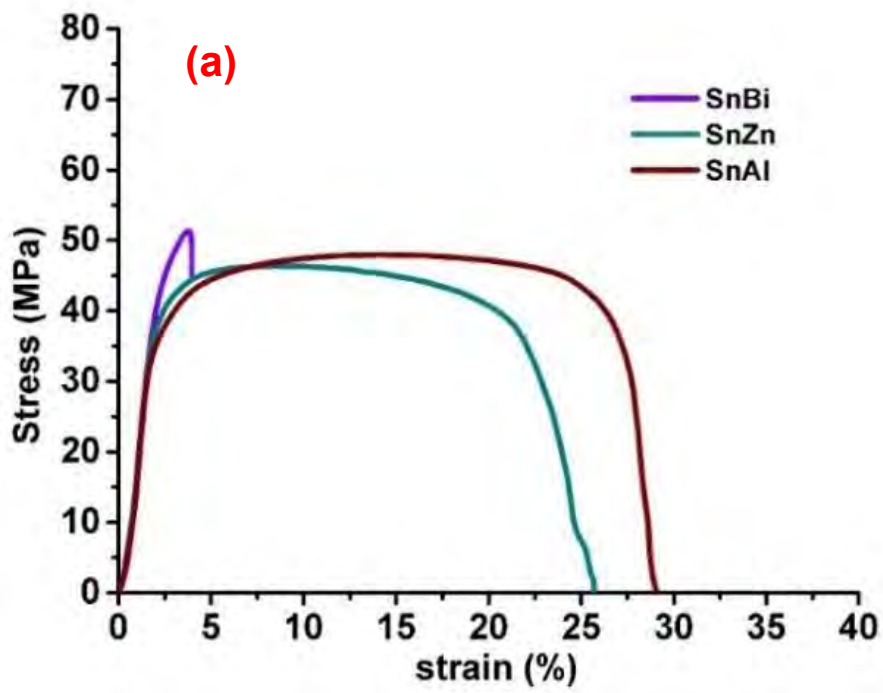
CHAPTER 5

CHARACTERIZATION OF MECHANICAL PROPERTIES

5.1 Stress-Strain Behaviour of the Alloys

Figure 5.1 shows the stress-strain plots under tension test for the various alloy systems at the different percentages of copper. The bismuth systems show the most brittle characteristics, that is the plastic part of the deformation is always less compared to other alloys at any percentage of copper doping. Bismuth alloys in general also show the lowest modulus of toughness among the alloys. The aluminium and zinc alloys on the other hand show somewhat similar values of toughness. At 0% copper doping, the binary sample of aluminium and tin has the highest modulus of toughness. At 0.1% doping the toughness of zinc is higher than that of the aluminium sample, the 0.3% plot also has the same trend for toughness and 0.5% reverts the trend back to that of the binary samples in that the aluminium has the greatest toughness.

The micrographs of the binary alloys show that, there is a distinct boundary region between the aluminium rich dendritic phase and the eutectic aluminium-tin phase. This grain boundary region maybe the reason why aluminium has higher toughness (energy storage due to deformation) as this boundary allows for greater deformation under tensile loads. While zinc system shows no such boundary region in between the eutectic and zinc rich phase leading to less deformation hence less toughness. At 0.1 and 0.3% of copper the formation of intermetallic compounds may push the aluminium specimens more towards the eutectic composition leading to the decreased values of toughness compared to zinc. At 0.5% the effect of increased IMCs on the aluminium specimen mainly manifests as an increase in the stresses generated while the change in elongation is minimal (from 22.5% to 21.5%). While the zinc system is affected much more with the excessive increase of IMC formation (coarsening microstructure), resulting in decrease in both the stress and deformation values leading in decreased toughness. The bismuth rich phase in the tin-bismuth alloys are inherently brittle and hence the bismuth alloys have the lowest plastic deformations.



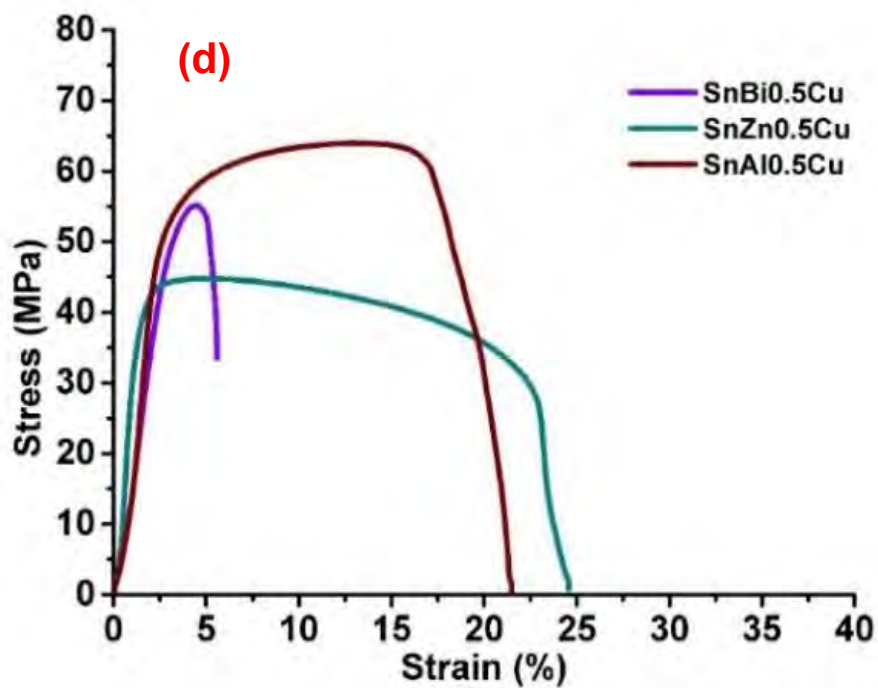
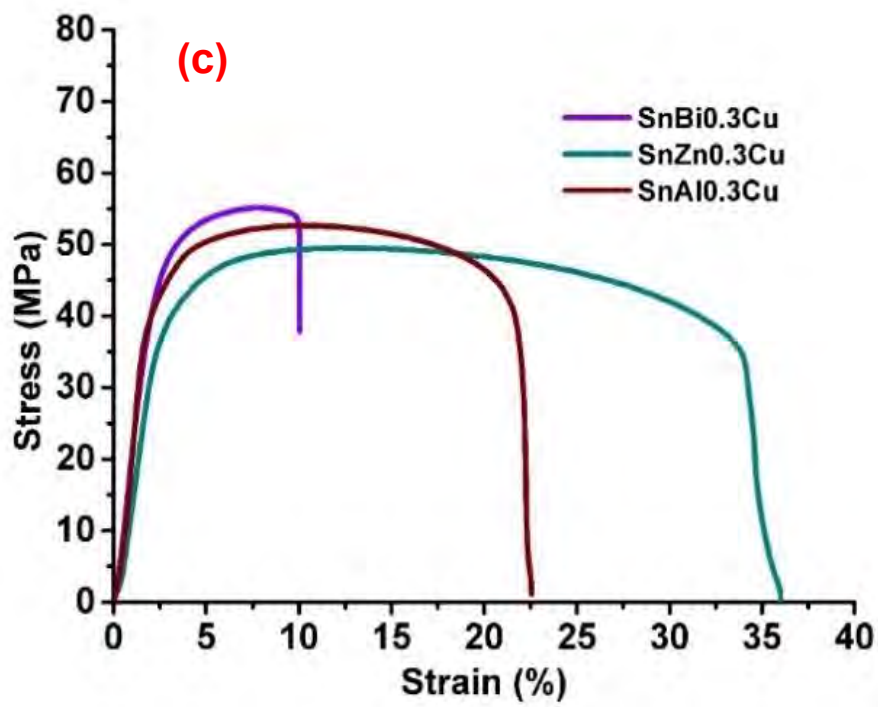


Figure 5. 1 Effect of Cu addition on the stress strain behaviour of the three binary solder systems(a) 0% wt. copper (b) 0.1% wt. copper (c) 0.3% wt. copper (d) 0.5% wt. copper

5.2 Tensile Properties

Figure 5.2 (a) compares the tensile strength of the different binary alloys systems. Among them the tin-bismuth composition has the greatest strength followed by tin-aluminium and tin-zinc systems. The fact that all the binary alloys show improved strength is also related to the refinement of their grain size and solid solution hardening. As stated earlier the presence of alternating eutectic layers in zinc and aluminium alloys mean that the grain size is reduced and grain boundary area is increased resulting in more resistance to dislocations. This increased resistance to displacement and deformation of the grains give rise to increased strength in the binary alloys. In the case of Sn-Bi alloy the strength increase is primarily due to solid solution hardening of Sn phase, though due to variations cooling conditions means that there will be some eutectic structure formation as well as will be seen later in the micrographs. While for the other alloys the solid solution phase is mostly pure tin (99% tin for aluminium alloy and 98% for zinc alloy)

Figure 5.2 (b) demonstrates the change in tensile strength of the alloy systems with addition of trace amounts of copper. For all the alloys addition of copper increases the tensile strength in general. For Sn-Bi system the increase is gradual (52 MPa at 0% Cu to about 55 MPa at 0.5% Cu) while for Sn-Zn systems a moderate increase (43 MPa at 0% Cu to about 58 MPa at 0.3% Cu) is noticed. Sn-Al system on the other hand shows a significant increase (48 MPa at 0% Cu 64 MPa at 0.5% Cu) in strength. It is also interesting to note that for the zinc system unlike other alloys the maximum tensile strength is not at 0.5% copper, rather it is at 0.3% copper.

The increase in tensile strength of the alloys is due to two main factors, due to intermetallic compound formation and the increase in eutectic phase in the microstructure. These intermetallic compounds have ionic/covalent bonds in addition to normal metallic bonds [68], this makes them hard and brittle with increased strength compared to the constituent elements [68], resulting in increased tensile strength for the samples. With the addition of copper, increasing amounts of intermetallic compounds between Cu and Sn, Al and Zn are formed for the Sn-Bi, Sn-Al and Sn-Zn alloys. Beyond a certain fraction of copper however, the increased IMC leads to a decrease in strength as at this point the volume fraction of IMCs will dominate the microstructure, making it very coarse. It is for this reason Sn-Zn alloy has a marked reduction in strength at 0.5%

copper. The formation of IMCs leads to grain size reduction which leads to increased tensile strength as well.

(a)

(b)

Figure 5. 2 (a) Mechanical Strength (Tensile Strength) of the three binary solder alloy systems, (b) Effect of Cu-addition on Tensile Strength

Figure 5.3(a) shows the maximum elongation of the binary alloys. Sn-Bi alloy is the most brittle in nature while the zinc and aluminium alloys have significantly higher elongation. The brittle behaviour of the bismuth system is due to the solid solution hardening of tin rich phase. That phase contains a higher concentration of solute (Bi) compared to the other alloys as a result is much more resistant to deformations. The tin rich phase in both the aluminium and zinc samples mostly have pure tin (Zn and Al are almost insoluble).

Figure 5.3(b) shows the effect of copper on the elongation at break for the three alloy systems. With increase in copper concentration all the alloys show decreasing elongation. For both the bismuth and zinc systems adding trace amounts of copper initially increases the elongation at break from the initial binary samples before decreasing with further addition of copper. The figure also indicates that, in general, at any composition of copper zinc alloy system has the highest elongation followed by the aluminium system and bismuth system.

As stated earlier with the increase of copper content, the formation of intermetallic compounds increases. This leads to the amount of eutectic composition increasing in the alloys. The eutectic composition with finer grain structure is then responsible for the decreased elongation which agrees with the previous graph for strength of alloys. Also, the intermetallic compounds themselves are hard brittle contributing to reduced deformations.

The nature of eutectic structure and the amount of IMC present in any given alloy sample along with the characteristics of the boundary and the distribution of these different phases is what determines the deformation characteristics of any alloy. For any given percentage of copper, the structure of eutectic region of zinc alloy is much more refined in nature while the structure for aluminium system is slightly more granular in nature, while bismuth has almost completely granular structure leading to zinc systems generally having larger values of elongations followed by aluminium and finally zinc. Taking a look into the aluminium and zinc system further reveals that the aluminium system has a distinct dendritic structure at any composition while zinc has long zinc rich needle like phases. These dendritic aluminium rich structures provide further resistance to deformations as well. The zinc rich phases while providing resistance to deformations

are not as strong as the aluminium dendrites. This leads the zinc systems to have higher elongation at any % of copper compared to the aluminium alloy system.

(a)

(b)

Figure 5. 3 (a) Elongation at break of the three binary solder alloy systems, (b) Effect of Cu-addition on Elongation at break

Figures 5.4(a) compare the elastic modulus of the constituent elements with binary alloys. From all the figures it can be seen that the binary alloys of bismuth, zinc and aluminium all show increased elastic modulus compared to pure tin. Figure 5.4(b) shows the change in the average young's modulus for all the alloy systems with increase in copper content. As expected in general with the increase in copper content the modulus of elasticity increases. All the alloys show a significant improvement up to 0.3% of copper, after which adding copper has no further significant improvement. One thing to note here is that the elastic modulus was calculated from the data which was directly and automatically recorded by the digital tensile test machine using a computer for all the as cast alloys, solidified under normal atmospheric conditions. No further modification on the data was performed by means of multiplying by correction factors or any other methods. Similar trends for the elastic modulus can be seen in the works of Kim et al. and Shen et al. [69,70]

The increase in elastic modulus of the binary alloys over pure tin is primarily due to the presence of the Bi/Zn/Al phase. Also, solid solution hardening due to diffusion of Bi/Zn/Al in to the Sn rich phase increases the modulus as well. Bi is most soluble in Sn resulting in Sn-Bi having high elastic modulus. The pure aluminium phase is what is responsible for highest elastic modulus of Sn-Al alloy. Elastic modulus primarily depends on the atomic bonding and packing of materials. With the increase in copper content, the atomic packing increases and there is increased formation of intermetallic compounds which have stronger covalent/ionic bonds than that of purely metallic bonds, resulting ever increasing values of elastic modulus.

(a)

(b)

Figure 5. 4 (a) Elastic modulus of the three binary solder alloy systems, (b) Effect of Cu-addition on elastic modulus.

5.3 Microhardness Characteristics

Figure 5.5(a) show the microhardness of the binary alloys. The hardness of all the binary alloys improves from that of pure tin. All three of the binary alloys show similar behaviour in terms of hardness. With the bismuth sample showing marginally higher hardness followed by aluminium and zinc alloys respectively.

Since microhardness is a measure of local deformation under point load, the nature of the structure of alloys and different characteristics of the phases present help to explain behaviour here. For bismuth the solid solution of Bi in Sn along with partial eutectic structure pushes the hardness marginally above that of the other two alloys. For Sn-Al alloy there is a dendritic presence of large aluminium rich crystals which leads to slightly decreased hardness. And for zinc large elongated needle like deposits of zinc in the eutectic structure decreases the hardness further.

Figure 5.5(b) Shows the effect of trace copper addition to the binary systems. In general, all the curves show an increase in hardness with increased copper addition. Though in the case of zinc system at 0.5% there is a decline with increased copper from previous composition. For any composition of copper aluminium system has the highest hardness followed by bismuth and lastly zinc systems.

As stated earlier with the addition of copper; tin, aluminium and bismuth are ejected from the previous structure to form intermetallic compounds. The hard and brittle nature of these scattered intermetallic compounds is what affects the mechanical properties along with the nature of the eutectic composition present in specimens. With the increase in copper the formation of IMCs increases which leads to increased hardness. In the case of aluminium system with addition of copper the long dendritic formations of aluminium crystals in the microstructure are broken up with scattered intermetallic compound formation between aluminium and copper. This phenomenon along with shifting of the initial composition towards the eutectic microstructure is what causes the aluminium system to increase in hardness the most. For bismuth system, doping with copper causes the formation of intermetallic compound between copper and tin leading to a shift towards the eutectic composition as well as growing the separate bismuth rich phase. With further increase in copper doping, the intermetallic compounds increase along with more uniform distribution of the bismuth rich phase as well as pushing the primary phase more towards the eutectic composition resulting in a more improved hardness

compared to zinc system. In the case of zinc system there is always a phase of zinc rich needles present which limit its hardness increase compared to other systems.

(a)

(b)

Figure 5. 5 (a) Microhardness of the three binary solder alloy systems, (b) Effect of Cu-addition on microhardness

(a)

(b)

Figure 5. 6 (a) Impact energy of the three binary solder alloy systems, (b) Effect of Cu-addition on impact energy

5.4 Impact Energy Characteristics

Figure 5.6(a) show the impact energy of the three binary alloys. As expected, the impact resistance for the binary bismuth system is much lower compared to other alloys. This is once again due to greater solid solution hardening in the Sn phase. Among the other two

alloys the impact energy should be similar as they both contain an Sn rich phase, however the other prominent phase in these consists of almost pure aluminium and zinc crystals as revealed in the microstructure and the difference in these two distinct phases is what manifests as the difference in impact energy for the aluminium and zinc alloys. Zinc has needle like elongated phases as a result with application of high strain rate impact loads these elongated crystals slip more easily while the microstructure of aluminium has long dendritic structure of crystals which are more inter locked with the eutectic phase resulting in more resistance to impact loads leading to higher energy absorption compared to zinc alloy.

Figure 5.6(b) highlights how the impact energy changes with copper content for the three alloy systems. With increase in copper content there is a reduction in energy absorption for all the alloy systems. For any composition the aluminium alloys show the best impact characteristics followed by zinc and finally bismuth systems. In the case of aluminium systems, it can be seen that up to 0.3% composition of copper the reduction in impact energy is gradual, after that there is a significant drop in impact energy. The zinc system shows a steadier drop from beginning to end. The bismuth system on the other hand shows the least drop in impact among all the alloy systems.

For the aluminium system, the presence of long dendritic aluminium rich crystals as will be seen later in the micrographs is what gives it increased impact resistance. The long dendritic structures interlock with the eutectic phase in essence preventing rupture when impact loads are applied. With the increase in copper content, the dendritic structures are broken up as intermetallic compounds are formed between aluminium and copper resulting in decrease in the impact energy. In the zinc alloys there are long, thin needle like zinc are present. During impact loads the presence of these zinc phases are what determine the energy absorbed. The higher the presence of this phase the greater the impact energy the alloy can absorb. With addition of copper this phase is reduced in the alloy as zinc and copper tend to form various intermetallic phases just like the previous aluminium alloys. And so, the energy absorbed gradually decreases. In the case of bismuth system, there are no such dendritic or needle like structures present. The phases present are the eutectic layers of β -Sn and Bi and a separate phase of Sn solid solution with significant Bi particles. And as such the impact energy is the lowest for this system as these phases are not able to resist impact loads like the one present in aluminium or zinc systems. With the increase of copper for bismuth system, tin is ejected from the previous composition

leading to the formation of intermetallic compounds between tin and copper which disrupt the eutectic structure resulting in a minor decrease in impact energy.

5.5 Comparison with Conventional Solders

The manufactured alloys specimens were compared on the basis of their mechanical characteristics. As expected, no single alloy had the most desirable properties among the specimens, instead the evaluation was done on a holistic approach. Over all the alloys which showed good mechanical characteristics were chosen for analysis against the commonly used Sn63Pb37 alloy and SAC305 alloy. As stated earlier these reference alloys were also manufactured using the same preparation methods as the bismuth, zinc and aluminium systems. That is, they are also naturally forming alloys, which have been left to cool down in ambient conditions and no other post processing or hardening or tempering method has been used. The mechanical, electrical and conduction characteristics of the manufactured reference alloys were also measured to compare with other values recorded in literature and justify their use. The table below shows these observed and recorded values.

Table 5. 1 Comparison of measured and literature values of mechanical properties of the conventional solders

Alloy name	UTS (MPa)	Elongation at break (%)	Hardness (Hv)	Conductivity (W/m.K)
Sn96.5Ag3Cu0.5 (SAC305)	Observed- 36.9	Observed- 52	Observed- 12.7	Observed-59
	Recorded- 38.69[71],26[72]	Recorded- 52.85 [71],35[72]	Recorded- 12[72],14[73]	Recorded- 57.8[74]
Sn63Pb37	Observed-36	Observed-53	Observed-7	Observed-51
	Recorded- 35[76]	Recorded- 33[76]	Recorded- 10.13[77]	Recorded- 50[75]

Comparing the experimental alloys with the conventional solder (Sn60Pb40) and the current favourite alternative SAC (305) yields some interesting results. Figure I compare the mechanical and conduction properties of the 0.3% doped copper alloy with as cast SAC305 and Sn60Pb40 alloys. Solder materials are used as interconnects in circuits and

in-between electronic components, and as such, they should have the ability to sustain sudden impact loads and not change shape which may lead to unwarranted contacts between components. Therefore, solder materials should have high hardness, elastic modulus and ultimate tensile strength along with moderate elongation. Among the bismuth alloys the binary composition has the highest strength however, it's extremely low elongation characteristics severely holds it back. Sn19.99Al0.1Cu alloy has higher ultimate tensile strength compared to SAC305. Also, it has moderate elongation, high hardness and comparable thermal conductivity but, it has significantly lower elastic modulus and impact characteristics. Sn19.99Zn0.1Cu is also another adequate alternative for SAC and tin-lead solders. It exhibits high tensile strength and hardness, sufficient elongation. Its conduction characteristics is also almost equal to SAC305 alloy, though it does have a lower modulus of elasticity and impact energy. It still however far exceeds the traditional Sn50Pb50 alloy on fronts. Sn19.94Al0.3Cu shows the best conduction characteristics while simultaneously having better tensile strength compared to both tin-lead and SAC solder. Aluminium specimens in general are better suited for high temperature solder applications as evidenced by the liquification temperatures for the binary alloys in table 3. On a holistic approach, Sn19.94Zn0.3Cu has shown the best characteristics and can be considered a suitable substitute to both SAC and tin-lead systems for low temperature soldering applications, as it is an improvement upon tin-lead alloy in almost every way while having the good elastic modulus, excellent ultimate strength, elongation and hardness characteristics. In addition to possessing good conduction and impact toughness characteristics. While the aluminium alloy containing 0.3% copper can be considered as a viable candidate for high temperature solder alloy.

Table 5. 2 Hardness and tensile properties of the binary and ternary alloys

Alloy Name	Elastic Modulus (GPa)	Ultimate Tensile Strength (MPa)	Elongation at break (%)	Microhardness (Hv)
Sn20Bi	1.831 ± 0.146	51.774 ± 3.2	5.000 ± 2.430	11.97 ± 0.719
Sn19.99Bi0.1Cu	2.357 ± 0.153	54.275 ± 2.68	19.432 ± 2.460	12.2 ± 0.969
Sn19.94Bi0.3Cu	2.530 ± 0.112	55.161 ± 2.215	10.0523 ± 2.401	12.55 ± 0.539
Sn19.9Bi0.5Cu	2.450 ± 0.251	55.770 ± 2.850	5.598 ± 2.870	13.15 ± 0.829
Sn20Zn	1.787 ± 0.107	43.162 ± 4.020	25.499 ± 3.565	11.51 ± 0.514
Sn19.99Zn0.1Cu	1.916 ± 0.177	47.442 ± 3.070	38.834 ± 2.436	11.97 ± 0.646
Sn19.94Zn0.3Cu	2.492 ± 0.121	49.563 ± 1.855	36.016 ± 2.086	12.2 ± 0.367
Sn19.9Zn0.5Cu	2.500 ± 0.210	44.838 ± 4.466	24.578 ± 3.500	11.88 ± 0.829
Sn20Al	1.865 ± 0.095	48.137 ± 2.675	30.019 ± 2.100	11.76 ± 0.734
Sn19.99Al0.1Cu	2.000 ± 0.181	52.658 ± 2.350	28.558 ± 2.569	12.87 ± 0.628
Sn19.94Al0.3Cu	2.687 ± 0.188	56.310 ± 3.500	22.559 ± 2.940	13.23 ± 0.895
Sn19.9Al0.5Cu	2.400 ± 0.1667	63.370 ± 4.000	21.498 ± 2.275	15.2 ± 0.807

Table 5. 3 Impact energy and thermal conductivity of the binary and ternary solder alloys

Alloy Name	Impact Energy(J)	Conductivity (W/m.K)
Sn20Bi	5.650 ± 2.22	25.28 ±1.862
Sn19.99Bi0.1Cu	3.728 ± 1.170	24 ±1.512
Sn19.94Bi0.3Cu	2.782 ± 1.500	32.63 ± 1.678
Sn19.9Bi0.5Cu	1.845 ± 1.100	19.25 ± 1.535
Sn20Zn	34.351 ± 2.555	47.52 ±1.712
Sn19.99Zn0.1Cu	19.031 ± 2.755	54.26 ± 1.957
Sn19.94Zn0.3Cu	10.600 ± 2.950	60 ± 1.717
Sn19.9Zn0.5Cu	7.116 ± 3.390	56.20 ±1.460
Sn20Al	57.595 ± 4.100	31.60 ±1.986
Sn19.99Al0.1Cu	56.297 ± 2.700	50.60 ± 2.034
Sn19.94Al0.3Cu	53.7 ± 3.200	74.90 ±2.704
Sn19.9Al0.5Cu	29.145 ± 3.000	50.57 ±1.565

SAC305	1	Sn63Pb37	2	Sn-Bi0.3Cu	3	Sn-Zn0.3Cu	4	Sn-Al0.3Cu	5
--------	---	----------	---	------------	---	------------	---	------------	---

Figure 5. 7 Comparison of major mechanical properties of the lead-free solder materials (with 0.3% *Cu* addition) with conventional *SAC305* and *Sn63Pb37* solders: (a) Tensile strength, (b) Elongation at break, (c) Microhardness, (d) Elastic Modulus, (e) Impact Energy, (f) Thermal Conductivity

CHAPTER- 6

CHARACTERIZATION OF ELECTROMAGNETIC PROPERTIES

The alloys were studied on the basis of their AC and DC characteristics. For AC analysis, the complex dielectric constant and complex permeability of the alloys were chosen. For DC analysis the bulk conductivity was chosen. The behaviour of each of the alloy systems were then explained in terms of their microstructural features. An estimate of the thermal conduction of the alloys were also made based on the electrical conductivity. The current alloys are also compared to commonly available SAC305 and Sn63Pb37 alloys on the basis of the same properties.

Before going further into the dielectric properties, it is first important to explain some of the modelling assumptions. The materials consist of highly resistive grain boundaries and highly conductive grains themselves. These grain boundaries act as spots for electron collision and scattering, while the electron clouds of the atoms inside the grains act as capacitors. In addition to the capacitive effects, the nuclei also act as dispersion zones. Considering all this the material as a whole can be modelled as an extremely leaky capacitor where the dispersion effects are represented by a resistance, the small capacitive effects of the atoms themselves are represented by an ideal capacitor connected in series. What makes conductive materials such as metals/metalloids different from other materials usually studied by impedance spectroscopy such as ceramics, electrochemical interfaces, protective coating is that the dispersive component is not negligible. In fact, the dispersive/ resistive effects in general are quite high.

Before conducting the impedance analyser measurements, the effect at the electrode-material interface was recognised. In order to mitigate the effects, all the samples were fine polished using similar techniques to insure similar surface roughness. Similar surface profiles mean the interface effects were similar for all the materials and hence played no significant role in the overall dielectric or impedance measures. Since the main interest is to compare the impedance characteristics of different test alloys with each other and the reference alloys, all the impedance plots were normalized with the impedance of the Sn63Pb37 alloy at 100 Hz.

$$\text{Relative Impedance } (\bar{z}) = \frac{Z_{\text{material}}}{Z_{\text{Sn63Pb37 at 100 Hz}}} \dots\dots\dots(6.1)$$

(a)

(b)

Figure 6. 1 (a) Bulk DC conductivity of the constituent elements and the binary alloys,
(b) Change in conductivity with copper content

6.1 Electrical Conductivity

Figure 6.1 (a) shows the conductivity of the constituent elements against the binary alloy. For the case of zinc alloy, the conductivity is improved compared to pure tin while for the bismuth system the conductivity of the binary alloy is lower than that of pure tin, which is expected as bismuth is the least conductive of all the metals resulting in a reduced conductivity of the binary mixture. However, the case of aluminum alloy is curious in that, even though aluminum has higher conductivity than tin, the resulting binary alloys actually shows reduced conductivity even compared to tin. This characteristic is related to the microstructure of the specimen. Figure 6.1 (b) illustrates the changes in electrical conductivity of the alloy with % of copper for the alloys. Electrical conductivity depends primarily on the distribution of the different phases, i.e., the distribution and alignment of the grains and on the nature and area of the boundaries [78,79,80]. The presence of intermetallic compounds also has an influence as well [81]. The conduction characteristics of the individual component alloys in this regard play no significant role in determining the overall conductivity of the finished alloy. The more organized the microstructure of the alloy, the better the conductivity of the alloy. From figure it can be seen that with addition of copper for both the zinc and aluminum system there is an increase in the conductivity. This is because in the case of both these systems with the addition of copper the microstructure is refined, grains are fairly in alignment and the boundary gaps between the grains are also reduced, even though there is an increase in the intermetallic compounds and an increase in grain boundary area. The increased grain boundary area and intermetallic compounds should actually reduce the conductivity of the specimen. The increased grain boundary area implies that there are increased number of crystalline regions whose boundaries should scatter electrons resulting in decreased conductivity. As for the Intermetallic compounds, they are non-conducting in nature due to the absence of metallic bonding. However, with increased copper doping the orientation of grains in space is improved. Meaning the gaps and sudden discontinuities among the grains is reduced which leads to an improvement in the conductivity. This is clearly evidenced in the case of the aluminum alloy, were at 0% copper there is a definite discontinuity between the aluminum rich phase and eutectic phase. However, with the increase in copper content this discontinuity is gradually reduced. This process continues up to 0.3% copper composition at which point the microstructure is most refined. After this point, further increase in copper content

increases the intermetallic phase in both the systems which is not suitable for electron conduction, hence the reduction in conductivity. For aluminum system the microstructure is more effected and so it undergoes a significant reduction in conductivity at 0.5% copper compared to zinc system. For bismuth the behavior plot is quite interesting. With the initial doping of copper at 0.1% there is a slight reduction in conductivity. This is because there is a marked increase in eutectic composition with segregated bismuth crystals which leads to reduction in conductivity due to increased grain boundary area. At 0.3% however, the conductivity is improved as the numerous small grains are reduced which helps to improve the conductivity in spite the formation of increased intermetallic compounds. At 0.5% doping, the Intermetallic compounds form at such a large extent that the conductivity is ultimately reduced.

(a)

(d)

(b)

(e)

(c)

(f)

Figure 6. 2 Frequency response of dielectric Properties of the constituent elements and binary alloys :(a-c) Dielectric Constant plots of Sn-Bi, Sn-Zn & Sn-Al binary alloys respectively, (d-f) Dielectric Loss plots of Sn-Zn & Sn-Al binary alloy

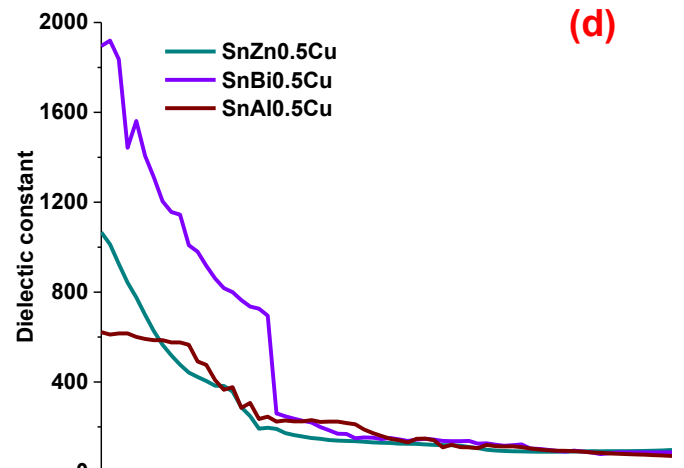
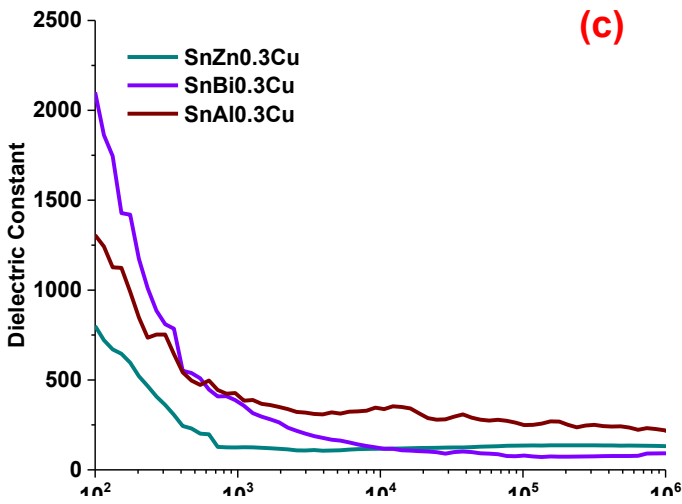
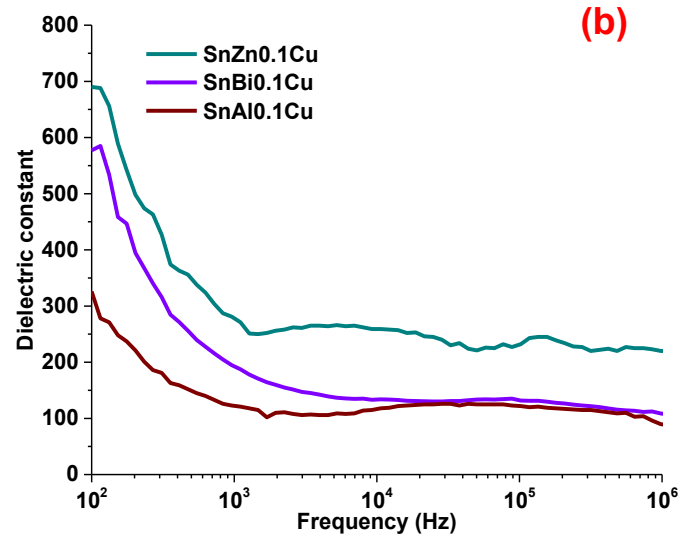
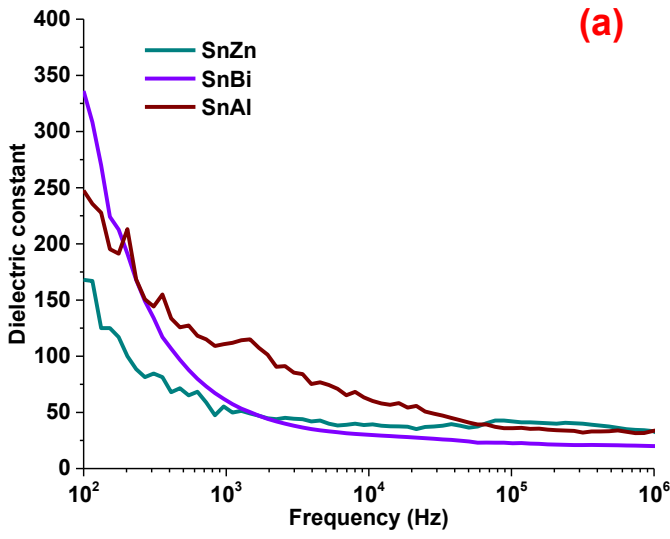


Figure 6. 3 Frequency response of dielectric constant for the alloys: (a) 0% wt. Cu, (b) 0.1% wt. Cu, (c) 0.3% wt. Cu and (d) 0.5% wt. Cu

(a)

(b)

(c)

(d)

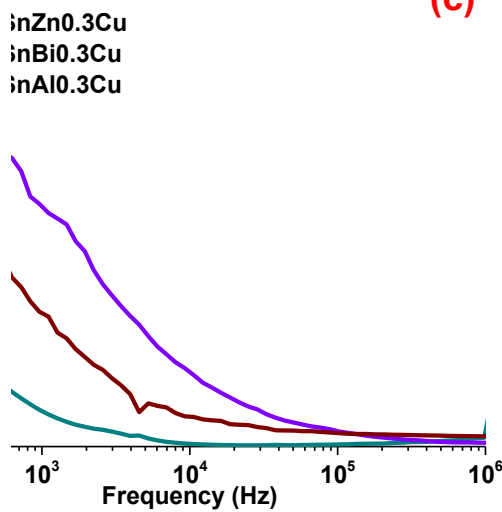


Figure 6. 4 Frequency response of dielectric loss for the alloys: (a) 0% wt. Cu, (b) 0.1%wt. Cu, (c) 0.3% wt. Cu and (d) 0.5% wt. Cu.

6.2 AC Dielectric Characteristics

The magnitude of dielectric function depends on the grain size and grain boundary area [82,83]. Were as the magnitude of the loss tangent in addition to grain size, boundary area is also dependent on the nature of the grain boundary region [84]. With the increase in copper content, all the alloys are shifted towards the eutectic region. As a consequence, significant increase in grain boundary area leading to increase in dielectric constant. As

for the dielectric loss, with increased doping of copper, there is formation of intermetallic phases. These phases are nonconductive (covalent/ionic bonds present instead of metallic bonds with free electrons) are in nature and act as further spots for dispersion as IMCs have high resistivity [85] and do not allow movement of electrons, not to mention the additional copper atoms themselves act as extra scattering point for the said electrons, which leads to a marked increase in dielectric loss for all the alloys. For these reasons, in figure 6.1 the dielectric constant of Sn80Zn20 is greater than both of its constituents while it has the lowest loss tangent. Both pure tin and zinc samples show higher loss tangents as their microstructures reveal much more discontinuous grain structure, especially the pure tin specimen. Pure bismuth has higher dielectric constant is much higher compared to both tin and tin-bismuth binary alloy, in terms of loss characteristics pure tin still shows significantly higher loss. Bismuth has much larger grains as seen from the micrographs hence its substantially higher dielectric constant with low loss tangent. While both the pure tin and binary alloy have much smaller grain sizes resulting in lower dielectric constant. The grain boundaries are much more spread out for pure tin leading to much higher losses. The numerous scattering points as evidenced by the micrograph of tin-bismuth binary alloy give it slightly higher loss tangent than pure bismuth. Among aluminum, tin and binary mixture of aluminum and tin, aluminum has the most refined microstructure as seen in the micrographs, and as a consequence both its dielectric function and loss characteristics are low compared to the other two materials. The binary Sn-Al mixture has large separated aluminum phases with a noticeable gap with the eutectic phase. These characteristics give it the highest dielectric function. Tin still has the highest dielectric constant as it still has significantly worse microstructure in the grain boundary region, and due to the presence of small separation between the eutectic tin-aluminum and aluminum rich phases in the binary alloy it has marginally higher loss characteristics compared to pure aluminum.

At 0% copper doping, observing the dielectric function and loss tangent curves indicates that overall aluminum has higher values of dielectric constant followed by zinc. While Bismuth does show high values of constant initially but, it drastically drops down to the lowest values even with the slightest increase in frequency. Taking a look at the microstructure leads to some clues about this behavior. In the case of aluminum there is a presence of large dendritic aluminum rich crystals which are spread out with a distinct boundary separating from the eutectic region. These large grains of aluminum with

separated boundaries are the reason why aluminum samples show higher values of dielectric constant. Similarly, in the zinc sample, there is a presence of almost pure zinc phase with tiny amounts of tin particles scattered throughout which look like needles. These large grains of zinc are the reason why zinc also has relatively higher values of dielectric constant compared to bismuth. Although in the case of the zinc system the size of these zinc deposits is smaller and there is no distinct separation between the zinc rich phase and eutectic phase compared to aluminum, which manifests as lower values compared to aluminum alloys. The loss characteristics are also tied to microstructure. The loss characteristics indicate the dispersion characteristics of the media, which is dependent on irregularities in the microstructure as these lead to more collisions of conduction electrons resulting in energy loss. For both bismuth and aluminum these irregularities are quite high leading to higher losses compared to zinc alloy. For aluminum alloy there is a distinct boundary that separates the aluminum and eutectic phases which leads to high losses. For the zinc system the grain boundary area is far less compared to other two alloys leading to lesser values of losses.

At 0.1% copper content the dielectric constant of zinc alloy is found to be the greatest followed by the bismuth and finally by the aluminum alloy. In the case of the dielectric loss, the bismuth alloy has noticeably higher loss factor compared to the other two alloys, which both show similar trend for the loss tangent curve. The high tangent loss of the bismuth alloy specimen indicates that it is a very dispersive sample, with many irregularities such as grain boundaries which result in energy loss of the electrons. This is also evident from the microstructure of the alloy which is shown later. The addition of copper leads to formation of intermetallic phases which reduce the percentage of tin in mixture and push the composition more towards the eutectic point. This increased push towards the eutectic point leads to grain size refinement with greater grain boundary area. This increased grain boundary act as regions for dispersion of electrons kinetic energy leading to high value of dielectric losses as well as contribution to overall dielectric function values, which is a combination of both dispersive and storage effects. Zinc alloy shows the highest dielectric constant but lower loss values indicate that the dispersion effects are less compared to bismuth alloys and the storage characteristics dominate the complex dielectric permittivity. Looking at the microstructure, here too there is a presence of long needle like zinc rich phases. Once again, these large zinc rich phases contribute to the high values of dielectric constant values. The addition of copper in the

zinc system induces the formation intermetallic phases between zinc and copper atoms. As a consequence, the amount of eutectic phase is increased resulting in grain boundary refinement leading which also lead to high values of dielectric constant as well.

At 0.3% copper doping bismuth alloy has the greatest dielectric constant followed by the aluminum alloy and finally zinc. The loss characteristics of the bismuth alloy is also the greatest followed by aluminum and finally by zinc alloy. The fact that both aluminum and bismuth alloys have high loss values indicate that both these alloys have small grains with high value of grain boundary area. Which can be seen from the photomicrographs later on. The formation of dark intermetallic phases is also noticed for both the alloys. The uneven distribution of these intermetallic compounds also lends themselves to increasing energy storage and loss characteristics as evident in increase in both dielectric constant and loss values. For the zinc system there is no significant change in the microstructure overall from that of the previous alloy at 0.1% of copper. The only noticeable change is that the long zinc rich phases have decreased slightly due to IMC formation between zinc and copper. These phases are once again distributed throughout the structure though much more uniformly compared to the other two alloys. The consequence being that this alloy has slightly higher dielectric function and loss compared to the zinc system at 0.1%Cu with the increase mostly being accounted for by the increase in dissipation characteristics.

When the trace copper is increased to 0.5%, The dielectric constant of the bismuth alloy shows the largest value followed by the zinc and finally by the aluminum alloy. Taking a look into the dielectric loss characteristics reveals that the bismuth alloy is the most dispersive media. Both the aluminum and zinc alloys are far less dispersive with lower loss tangent values. Taking a look into the microstructure shows that even though all three alloys have increased formation of intermetallic compounds, the effects of copper doping are more pronounced in the case of the bismuth alloy. This can be seen in the photomicrographs as increased dark regions. This increased IMC phase contributes to higher energy dissipation behavior. In the case of the other alloys the presence of aluminum rich and zinc rich large crystals is what dominate the dielectric behavior. These large grains ensure that the real part of the dielectric function is much more prominent compared to the bismuth alloy. Hence showing less loss characteristics.

Figure 6.5 and 6.6 show the variation of impedance with frequency. With increase in frequency there is a reduction in dielectric function. This is because at higher frequencies the characteristic time or the characteristic frequency of the different polarization mechanism and the characteristic frequency for the electron collisions with the lattice points is exceeded by the applied alternating field frequency. And since the impedance characteristics are a combination of this dielectric effect and DC resistivity, at higher frequencies it reduces to DC conductivity. Also taking a look at the impedance plots reveals that at any composition of copper, the impedance plots follow the dielectric constant plots, this is to be expected as described earlier, impedance is just the sum of complex resistance and dc resistance at any frequency.

(a)

(b)

(c)

Figure 6. 5 Impedance vs frequency plots of the constituent elements and the binary alloys: (a)Sn-Bi alloy, (b)Sn-Zn alloy and (c) Sn-Al alloy

(a)

(b)

(c)

(d)

Figure 6. 6 Impedance vs frequency of the alloy samples: (a) 0 % wt. Cu, (b) 0.1% wt. Cu, (c) 0.3% wt. Cu and (d) 0.5% wt. Cu

6.3 AC Magnetic Characteristics

From (figures 6.7 and 6.8) all the permeability plots it is evident that all the alloys are highly paramagnetic as the real part of the permeability is very close to unity. The implications of having low real part of the complex permeability are that it indicates that all the alloys are hard magnetic material and when introduced to external magnetic fields the tendency of the said alloys in question is not to store any energy. However, when looking at the imaginary part of the permeability the scenario is quite different. All the alloys have imaginary part in the thousands indicating a significant time lag between the magnetic domains and the external field. This also indicates the lossy characteristics of the alloys in question. The alloys will have significant energy loss characteristics. The aluminium specimens always show slightly lower values for the imaginary part of the complex permeability indicating less thermal heating effects compared to other alloys. As to the reason why the real part of the permeability of the alloys follows this trend is related to two factors. Firstly, all the constituent elements of the alloys are primarily paramagnetic and diamagnetic in nature, second is the presence of intermetallic compounds in the alloys. These IMC phases themselves are themselves highly paramagnetic in nature. Taking a look into the plots also reveals that type of dispersion present here is relaxation type. No resonance type dispersion characteristics were present. The primary means of energy dispersion in the specimens is by spin rotation, that is the lag time between the applied field and the orientation of the magnetic domains in the applied field direction [86]. No domain growth in the applied field direction is present here. Since domain wall motion type resonance is absent, it means that the loss characteristics in this regard have no direct relation with the microstructure (grain size) of the materials [86].

(a)

(d)

(b)

(e)

(c)

(f)

Figure 6. 7 Frequency response of the relative permeability of the constituent elements and the corresponding binary alloys: (a) SnBi and its constituents, (b) SnAl and its constituents, (c) SnZn and its constituents

(a1)

(a2)

(b1)

(b2)

(c1)

(c2)

(d1)

(d2)

Figure 6. 8 Frequency response of relative permeability of the solder alloy systems: (a1) Real part at 0% wt. Cu (a2) Imaginary part at 0% wt. Cu (b1) Real part at 0.1% wt. Cu (b2) Imaginary part at 0.1% wt. Cu (c1) Real part at 0.3% wt. Cu (c2) Imaginary part at 0.3% wt. Cu (d1) Real part 0.5% wt. Cu

6.4 Estimation of Thermal Conductivity of the Solder Materials from Bulk DC Conductivity

Table 6. 6 Estimated thermal conductivity of the solder materials

Specimen	Thermal Conductivity (W/m.K)
Sn	36.00 ±1.439
Bi	11.00 ±1.277
Zn	75.00 ±2.044
Al	200.00 ±9.856
Sn20Bi	25.28 ±1.861
Sn19.99Bi0.1Cu	24 ±1.512
Sn19.94Bi0.3Cu	32.63 ± 1.678
Sn19.9Bi0.5Cu	19.25 ± 1.535
Sn20Zn	47.52 ±1.712
Sn19.99Zn0.1Cu	54.26 ± 1.957
Sn19.94Zn0.3Cu	60 ± 1.717
Sn19.9Zn0.5Cu	56.20 ±1.460
Sn20Al	31.60 ±1.986
Sn19.99Al0.1Cu	50.60 ± 2.034
Sn19.94Al0.3Cu	74.90 ±2.704
Sn19.9Al0.5Cu	50.57 ±1.565

Table 6.1 estimates the thermal conductivity of the solder materials on the basis of electrical conduction characteristics. In metals and alloys both electrical and thermal conductivity are closely related to each other as both are determined by free electron motion inside the material. The Wiedemann–Franz Law relates these two quantities. It states that, the ratio of the electronic contribution of the thermal conductivity κ to the electrical conductivity σ of a metal is proportional to the temperature T based on a semi-

classical treatment of the electron gas [87,88]. The proportionality constant via which these two are related is known as Lorenz number (L_0). According to the free electron or electron gas model is $2.445 \times 10^{-8} \text{ W} \cdot \Omega / \text{K}^2$. However, in real metals and alloys the electrons are not totally free from the influence of nucleus, so the value for Lorenz number for real systems varies, all be it very acutely from material to material. The values of L_0 for pure tin and bismuth are 2.45 and 3.10 respectively [89]. For the alloy of Sn0.25Al the number was found to be 2.42 [56] which is close to the theoretical value of 2.445. For tin-zinc systems the values were also close to that of 2.45 [50]. Though the thermal conductivity also has a contribution from phonons, in most cases it can be neglected as in metals and binary alloys the primary mechanism of heat and charge transfer is by means of electrons only. Here the Lorenz number of tin was taken to estimate the thermal conductivity of the alloys as tin is the primary component and as can be seen from previous discussion the value doesn't change significantly between systems. The Wiedemann–Franz law for a specific metal is given below.

$$\kappa = L \cdot T \cdot \sigma \dots\dots\dots(6.2)$$

Were, κ = Thermal conductivity of the material (W/m.K)

L = Lorenz number for the specific material ($\text{W} \cdot \Omega / \text{K}^2$)

σ = Bulk electric conductivity of the material ($\Omega^{-1} \cdot \text{m}^{-1}$)

T = Temperature of the bulk conductivity measurements (K)

Like electrical conductivity, thermal conductivity depends primarily on the distribution of the different phases, i.e., the distribution and alignment of the grains and on the nature and area of the boundaries. Intermetallic compounds have a role to play as well. In this case, the conduction characteristics of the individual component alloys have no bearing on the overall conductivity of the finished alloy. The greater the alloy's electrical and thermal conductivity, the more organized its microstructure is. The addition of copper to both the zinc and aluminium systems increases both the thermal and electrical conductivity, as seen in the figure. This is because, with the addition of copper to each of these systems, the microstructure is optimized, grains are more evenly aligned, and grain boundary gaps are minimized, despite an increase in intermetallic compounds and grain boundary area. The increased grain boundary area and intermetallic compounds should actually reduce the two conductivities of the specimen. Because of the larger grain boundary area, there are more crystalline regions whose boundaries can disperse electrons, resulting in lower conductivity. Intermetallic materials, on the other hand, are non-conducting due to the lack of metallic bonding. Increased copper doping, on the other

hand, improves grain orientation in space. The gaps and abrupt discontinuities between the grains are minimized, resulting in an increase in conductivity. This is clearly shown in the case of the aluminium alloy, where there is a distinct discontinuity between the aluminium rich phase and the eutectic phase at 0% copper. This discontinuity, however, is steadily reduced as the copper content rises. This process is repeated until the copper content reaches 0.3 percent, at which stage the microstructure is most refined. Further increases in copper content after this point increase the intermetallic step in both systems, which is not conducive to electron movement, resulting in a decrease in conductivity. In comparison to the zinc system, the microstructure of the aluminium system is more effected, resulting in a major decrease in conductivity at 0.5 percent copper. The behaviour plot for bismuth is very interesting. There is a small decrease in conductivities when copper is doped at 0.1 percent. This is because there is a marked increase in eutectic composition with segregated bismuth crystals which leads to reduction in conductivities due to increased grain boundary area. The conductivities improve at 0.3 percent because the number of small grains is decreased, which tends to improve the conductivity despite the creation of more intermetallic compounds. Intermetallic compounds form to such a large degree at 0.5 percent doping that both the electric and thermal conductivity is reduced.

6.5 Comparison with Commonly used Solders

Figure 6. 9 Comparison of electrical characteristics of the solder samples with those of conventional solders

Figure 6. 10 Comparison of magnetic permeability characteristics of the solder samples with those of conventional solders

In this section one of the copper compositions is chosen for comparison against conventional SAC305 and Sn63Pb37 alloy synthesized under same conditions as the test alloys. All of the AC and DC properties are compared against each other. The 0.3% copper composition was found to have the best properties among the experimental alloy so it was selected for analysis against the conventional alloys.

From figure 18 it can be seen that the aluminum alloy at 0.3% composition had the least resistivity of all the test alloys, while having reasonably good dielectric characteristics. Therefore, it can be a potential soldering alloy candidate and compared against SAC305 and Sn63Pb37. The only drawback being it requires somewhat of an elevated temperature to melt. All the test alloys are better in terms of magnetic characteristics when compared against traditional alloys. For dielectric behavior, both zinc and aluminum alloy have comparable dielectric constant and loss to the reference alloys. Impedance of the aluminum alloy is close to that of the reference alloys while the bulk conductivity of the aluminum alloy is significantly better than that of SAC305 and Sn-Pb alloy. The 0.3% zinc alloy also has many desirable qualities in terms of DC and AC properties. It has comparable resistivity to the SAC and aluminum alloys However, it shows significantly higher impedance compared to all other materials.

CHAPTER-7

CONCLUSIONS AND RECOMMENDATIONS

7.1 Conclusions

In an attempt to find a suitable alternative to lead-free soldering material, a new comparative analysis of mechanical and electromagnetic characteristics has been carried out with three potential tin-based binary alloy systems under the influence of trace addition of copper. More specifically, *Sn-Bi*, *Sn-Zn* and *Sn-Al* binary systems are investigated experimentally for their major mechanical, electrical (both DC and AC responses) and AC magnetic behaviours as a function of trace addition (0 ~ 0.5% wt.) of copper. All the binary and ternary alloy materials are casted with identical proportion of base materials, that is, 80%*Sn* and 20%*x*, where $x = Bi/Zn/Al$, under normal atmospheric condition. A large number of standard test samples are prepared from the cast materials for the direct measurement of major mechanical, electrical, magnetic as well as microstructural properties, which include standard tension test, microhardness and impact toughness tests, measurement of DC electrical conductivity, test of AC impedance, dielectric constant and loss as a function of operating frequency, measurements of AC magnetic permeability, etc. Optical and Scanning Electron Microscopy (SEM) are also adopted to capture the microstructural images of the solder systems, together with the Energy Dispersive X-ray Spectroscopy to enable the associated compositional/elemental analysis. Finally, the observed functional properties of all the test samples are compared with those of traditional lead-solder (*Sn63Pb37*) as well as one of the conventional lead-free solders in use (*SAC305*). The major findings of the present investigation can be concluded as follows:

1. In general, with the increase in copper percentage, the strength and hardness increase for all the alloys, while elongation and impact energy decrease due to the formation of IMCs and refinement of eutectic microstructures.
2. Taking all the mechanical properties into account, it is realized that the aluminium and zinc systems are highly attractive in terms of their major mechanical properties. More critical analysis of the properties reveals that the aluminium-based solder is possessing better properties compared to those of zinc-based solder.

3. However, taking the soldering as well as operational temperatures into account, the zinc system is more suited for conventional soldering (low-temperature soldering) applications. Specifically, the composition doped with 0.3% of copper showed good tensile strength, excellent elongation at break, good microhardness and impact energy absorption characteristics.
4. The aluminium system can be used in high temperature soldering application as it has higher melting temperatures. The tin-aluminium system with 0.1/0.3% copper can be an attractive candidate in this regard.
5. Addition of copper causes a negative effect in terms of dielectric properties, which increases both the relative permittivity and dielectric loss characteristics. It is thus realized that increase in copper basically increases the energy storage and energy loss characteristics for the alloys.
6. All the alloys show negligible real part of relative magnetic permeability regardless of the copper content. This is probably due to the fact that all the constituent elements used in the alloy systems are all diamagnetic (bismuth) or slightly paramagnetic.
7. The DC electrical conductivity characteristics of all the alloys, on the other hand, are found to depend on IMCs present in the alloys as well as the distribution and refinement of the microstructure. As a result, up to a certain amount of copper, the conductivity increases.
8. Therefore, taking all the characteristics into account, the zinc and aluminium solder systems containing 0.3% copper show overall better performance for conventional low-temperature and high-temperature soldering, respectively, thereby verifying them as suitable alternatives to lead-free soldering of modern electronic devices.

7.2 Recommendations

In this experimental investigation the three different solder alloy systems were compared with each other on the basis of their mechanical, bulk electrical and AC electric and magnetic characteristics. The comparison was quite thorough as all of the important aspects of each solder material was analysed and compared to each other. Nevertheless,

during the course of this investigating, a number of new research scopes also presented themselves, they are:

1. The present research is basically concerned with as cast, naturally formed alloys. However, the effect of different processing parameters and treatment methods, such as, different cooling rates, heat treatments may also have a significant impact on the properties of alloys and thus can be investigated.
2. The present investigation suggests that *Sn-Al* alloys can be an attractive candidate for high temperature soldering due to their low cost and good thermal, mechanical and electromagnetic characteristics. However, no serious attempts have so far been made to suggest a specific solution of composition for this alloy. So, a future investigation focusing solely on the *Sn-Al* system with a wider range of copper addition can be of great practical importance.
3. The main focus of this work was on the characterization of the bulk solder alloys. But solder materials are used as electrical interconnects for joining similar or dissimilar conductive materials. These solder joints are often subjected to different types of loads and thermal conditions in addition to conduction of current. Therefore, a possible new research can be devised focusing on the performance evaluation of the above solder alloys as a joining material of conductors under current flow.

REFERENCES

- [1] Hong YK, Lee J. Ferrites for RF passive devices. *Solid State Physics*. 2013; 64:237-329.
- [2] El-Ashram T. Structure and properties of rapidly solidified pure tin. *Radiation Effects & Defects in Solids*. 2006;161(3):193-7.
- [3] Naidich YV, Taranets NY. Wettability of aluminium nitride by tin–aluminium melts. *Journal of materials science*. 1998;33(15):3993-7.
- [4] Peng W. An investigation of Sn pest in pure Sn and Sn-based solders. *Microelectronics Reliability*. 2009;49(1):86-91.
- [5] Musgrave MJ. On the relation between grey and white tin (α -Sn and β -Sn). *Proceedings of the Royal Society of London. Series A. Mathematical and Physical Sciences*. 1963;272(1351):503-28.
- [6] Brusse J, Ewell G, Siplon J. Tin whiskers: Attributes and mitigation. *Carts Europe*. 2002;16.
- [7] Islam RA, Chan YC, Jillek W, Islam S. Comparative study of wetting behavior and mechanical properties (microhardness) of Sn–Zn and Sn–Pb solders. *Microelectronics Journal*. 2006;37(8):705-13.
- [8] Hua F, Mei Z, Glazer J. Eutectic Sn–Bi as an alternative to Pb-free solders. In 1998 Proceedings. 48th Electronic Components and Technology Conference (Cat. No. 98CH36206) 1998 (pp. 277-283). IEEE.
- [9] Shohji I, Yoshida T, Takahashi T, Hioki S. Comparison of low-melting lead-free solders in tensile properties with Sn–Pb eutectic solder. *Journal of Materials Science: Materials in Electronics*. 2004;15(4):219-23.
- [10] Yu XY, Xing WQ, Ding M. Ultrasonic semi-solid coating soldering 6061 aluminum alloys with Sn–Pb–Zn alloys. *Ultrasonics sonochemistry*. 2016; 31:216-21.
- [11] Min D. Joining of 6061 aluminium ultrasonic soldered of Sn–Pb–Zn alloys. *Materials Science and Technology*. 2013;29(3):342-5.
- [12] Li K, Lin J, Wang T, Lei Y, Fu H. Effects of Ge on Microstructure, Spreadability, and Mechanical Properties of the Sn-32Pb-18Cd Solder Alloy. *Journal of Materials Engineering and Performance*. 2020;29(7):4541-8.
- [13] Ding Y, Wu GD, Wang XL, Yan GS, Hang CJ. Tensile testing and microstructure analysis on Sn–Pb–Cd and Sn–Pb eutectic solder. In 2014 15th International Conference on Electronic Packaging Technology 2014 (pp. 893-897). IEEE.
- [14] Anderson IE and Terpstra RL. Lead-free solder. US Patent No. US6231691B1, May 15, 2001.
- [15] Cheng S, Huang CM, Pecht M. A review of lead-free solders for electronics applications. *Microelectronics Reliability*. 2017; 75:77-95.
- [16] Kang H, Rajendran SH, Jung JP. Low Melting Temperature Sn–Bi Solder: Effect of Alloying and Nanoparticle Addition on the Microstructural, Thermal, Interfacial Bonding, and Mechanical Characteristics. *Metals*. 2021;11(2):364.

- [17] Liu JC, Zhang G, Ma JS, Suganuma K. Ti addition to enhance corrosion resistance of Sn–Zn solder alloy by tailoring microstructure. *Journal of Alloys and Compounds*. 2015; 644:113-8.
- [18] Chidambaram V, Hattel J, Hald J. Design of lead-free candidate alloys for high-temperature soldering based on the Au–Sn system. *Materials & design*. 2010 ;31(10):4638-45.
- [19] Khodabakhshi F, Zareghomsheh M, Khatibi G. Nanoindentation creep properties of lead-free nanocomposite solders reinforced by modified carbon nanotubes. *Materials Science and Engineering: A*. 2020; 797:140203.
- [20] Lee CJ, Min KD, Park HJ, Jung SB. Mechanical properties of Sn-58 wt% Bi solder containing Ag-decorated MWCNT with thermal aging tests. *Journal of Alloys and Compounds*. 2020; 820:153077.
- [21] Yang Z, Zhou W, Wu P. Effects of Ni-coated carbon nanotubes addition on the electromigration of Sn–Ag–Cu solder joints. *Journal of alloys and compounds*. 2013; 581:202-5.
- [22] McCormack M, Jin S, Kammlott GW, Chen HS. New Pb-free solder alloy with superior mechanical properties. *Applied Physics Letters*. 1993;63(1):15-7.
- [23] Kariya Y, Otsuka M. Effect of bismuth on the isothermal fatigue properties of Sn-3.5 mass% Ag solder alloy. *Journal of Electronic Materials*. 1998;27(7):866-70.
- [24] Chen SW, Lee SW, Yip MC. Mechanical properties and intermetallic compound formation at the Sn/Ni and Sn-0.7 wt.% Cu/Ni joints. *Journal of Electronic Materials*. 2003;32(11):1284-9.
- [25] Quan L, Frear D, Grivas D, Morris JW. Tensile behavior of Pb-Sn solder/Cu joints. *Journal of Electronic Materials*. 1987;16(3):203-8.
- [26] Islam RA, Wu BY, Alam MO, Chan YC, Jillek W. Investigations on microhardness of Sn–Zn based lead-free solder alloys as replacement of Sn–Pb solder. *Journal of alloys and compounds*. 2005;392(1-2):149-58.
- [27] Gain AK, Chan YC, Yung WK. Microstructure, thermal analysis and hardness of a Sn–Ag–Cu–1 wt% nano-TiO₂ composite solder on flexible ball grid array substrates. *Microelectronics Reliability*. 2011;51(5):975-84.
- [28] Yang L, Zhou W, Ma Y, Li X, Liang Y, Cui W, Wu P. Effects of Ni addition on mechanical properties of Sn58Bi solder alloy during solid-state aging. *Materials Science and Engineering: A*. 2016; 667:368-75
- [29] Han YD, Jing HY, Nai SM, Xu LY, Tan CM, Wei J. Temperature dependence of creep and hardness of Sn-Ag-Cu lead-free solder. *Journal of Electronic Materials*. 2010 ;39(2):223-9.
- [30] Shang JK, Zeng QL, Zhang L, Zhu QS. Mechanical fatigue of Sn-rich Pb-free solder alloys. In *Lead-Free Electronic Solders 2006* (pp. 211-227). Springer, Boston, MA.

- [31] Mattila TT, Kivilahti JK. The Failure Mechanism of Recrystallization–Assisted Cracking of Solder Interconnections. Chapter. 2012 Mar 7; 8:179-206.
- [32] Reid M, Punch J, Collins M, Ryan C. Effect of Ag content on the microstructure of Sn-Ag-Cu based solder alloys. *Soldering & Surface Mount Technology*. 2008 Sep 19.
- [33] Jung DH, Jung JP. Review of the wettability of solder with a wetting balance test for recent advanced microelectronic packaging. *Critical Reviews in Solid State and Materials Sciences*. 2019;44(4):324-43.
- [34] Prabhu KN. Reactive wetting, evolution of interfacial and bulk IMCs and their effect on mechanical properties of eutectic Sn–Cu solder alloy. *Advances in colloid and interface science*. 2011;166(1-2):87-118.
- [35] Arenas MF, Acoff VL. Contact angle measurements of Sn-Ag and Sn-Cu lead-free solders on copper substrates. *Journal of Electronic Materials*. 2004;33(12):1452-8.
- [36] Sona M, Prabhu KN. Effect of reflow time on wetting behavior, microstructure evolution, and joint strength of Sn-2.5 Ag-0.5 Cu solder on bare and nickel-coated copper substrates. *Journal of Electronic Materials*. 2016;45(7):3744-58.
- [37] Rodrigues N, Ferreira AC, Teixeira SF, Soares D, Teixeira JC, Cerqueira F, Macedo F. Contact angle measurement of SAC 305 solder: numerical and experimental approach. *Journal of Materials Science: Materials in Electronics*. 2016;27(9):8941-50.
- [38] Sharma A, Sohn HR, Jung JP. Effect of graphene nanoplatelets on wetting, microstructure, and tensile characteristics of Sn-3.0 Ag-0.5 Cu (SAC) alloy. *Metallurgical and Materials Transactions A*. 2016;47(1):494-503.
- [39] Wang Y, Wang G, Song K, Zhang K. Effect of Ni addition on the wettability and microstructure of Sn₂. 5Ag₀. 7Cu₀. 1RE solder alloy. *Materials & Design*. 2017; 119:219-24.
- [40] Zhang R, Cai J, Wang Q, Li J, Hu Y, Du H, Li L. Thermal resistance analysis of Sn-Bi solder paste used as thermal interface material for power electronics applications. *Journal of Electronic Packaging*. 2014;136(1):011012.
- [41] Silva BL, Cheung N, Garcia A, Spinelli JE. Evaluation of solder/substrate thermal conductance and wetting angle of Sn–0.7 wt% Cu–(0–0.1 wt% Ni) solder alloys. *Materials Letters*. 2015; 142:163-7.
- [42] Basaran C, Chandaroy R. Mechanics of Pb40/Sn60 near-eutectic solder alloys subjected to vibrations. *Applied Mathematical Modelling*. 1998;22(8):601-27.
- [43] Song JM, Chang YL, Lui TS, Chen LH. Vibration fracture behavior of Sn-Bi solder alloys with various Bi contents. *Materials transactions*. 2004;45(3):666-72.

- [44] Song JM, Lui TS, Chang YL, Chen LH. Effect of Zn content on the vibration fracture behavior of Sn-Zn and Sn-Zn-Bi solders. *Journal of electronic materials*. 2006 ;35(5):929-36.
- [45] Liu B, Guo F. Electrical conductivity changes of bulk tin and Sn-3.0Ag-0.5Cu in bulk and in joints during isothermal aging. *International Journal of Minerals, Metallurgy, and Materials*. 2010; 17(4): 453–458.
- [46] Amin NA, Shnawah DA, Said SM, Sabri MF, Arof H. Effect of Ag content and the minor alloying element Fe on the electrical resistivity of Sn–Ag–Cu solder alloy. *Journal of alloys and compounds*. 2014; 599:114-20.
- [47] Yakymovych A, Plevachuk Y, Švec P, Janičkovič D, Šebo P, Beronska N, Nosko M, Orovcik L, Roshanghias A, Ipser H. Nanocomposite SAC solders: morphology, electrical and mechanical properties of Sn–3.8 Ag–0.7 Cu solders by adding Co nanoparticles. *Journal of Materials Science: Materials in Electronics*. 2017;28(15):10965-73.
- [48] Çadırılı E, Şahin M, Kayalı R, Arı M, Durmuş S. Dependence of electrical and thermal conductivity on temperature in directionally solidified Sn–3.5 wt% Ag eutectic alloy. *Journal of Materials Science: Materials in Electronics*. 2011;22(11):1709-14.
- [49] Ari ME, Saatçi BU, Gündüz M, Payveren M, Durmuş S. Thermo-electrical characterization of Sn–Zn alloys. *Materials characterization*. 2008;59(6):757-63.
- [50] Plevachuk Y, Sklyarchuk V, Svec P, Janickovic D, Illekova E, Yakymovych A. Thermophysical structure-sensitive properties of Tin–Zinc alloys. *Journal of Materials Science: Materials in Electronics*. 2017;28(1):750-9.
- [51] Gancarz T, Fima P, Pstruś J. Thermal expansion, electrical resistivity, and spreading area of Sn-Zn-In alloys. *Journal of materials engineering and performance*. 2014;23(5):1524-9.
- [52] Gancarz T, Pstruś J. Characteristics of Sn-Zn cast alloys with the addition of Ag and Cu. *Archives of Metallurgy and Materials*. 2015;60(3):1603-8.
- [53] Chen KJ, Hung FY, Lui TS, Hsu L. Low Conductivity Decay of Sn–0.7 Cu–0.2 Zn Photovoltaic Ribbons for Solar Cell Application. *Micromachines*. 2019;10(8):550.
- [54] Kumar MR, Behera CK, Mohan S. Measurement of Electrical Properties of Sn-Bi-In Alloys. *Journal of Electronic Materials*. 2019;48(10):6561-9.
- [55] Flores FU, Seidman DN, Dunand DC, Vo N.Q. (2018) Development of High-Strength and High-Electrical-Conductivity Aluminum Alloys for Power Transmission Conductors. In: Martin O. (eds) *Light Metals 2018*. TMS 2018. The Minerals, Metals & Materials Series. Springer, Cham
- [56] Tezel FM, Saatçi B, Arı M, Acer SD and Altuner E. Structural and thermo-electrical properties of Sn–Al alloys. *Applied Physics A*. 2016; 122(10): 906.

- [57] Guo F, Lee JG, Hogan T, Subramanian KN. Electrical conductivity changes in bulk Sn, and eutectic Sn-Ag in bulk and in joints, from aging and thermal shock. *Journal of materials research*. 2005;20(2):364-74.
- [58] Kang SK, Choi WK, Yim MJ, Shih DY. Studies of the mechanical and electrical properties of lead-free solder joints. *Journal of Electronic Materials*. 2002;31(11):1292-303.
- [59] Cook BA, Anderson IE, Haringa JL, Terpstra RL. Effect of heat treatment on the electrical resistivity of near-eutectic Sn-Ag-Cu Pb-free solder alloys. *Journal of electronic materials*. 2002;31(11):1190-4.
- [60] Sonawane PD, Bupesh Raja VK, Gupta M. Microstructure, Mechanical, and Electrical Properties and Corrosion Analysis of Lead-Free Solder CSI Joints on Cu Substrate Using Novel Concentrated Solar Energy Soldering (CSES) Method. *Advances in Materials Science and Engineering*. 2020 ;2020.
- [61] Cheng J, Hu X, Li Q. Effects of the Ni electrodeposit on microstructure evolution and electrical resistance of the P-type Bi₂Te₃ solder joint. *Journal of Alloys and Compounds*. 2020; 832:155006.
- [62] Ismail N, Jalar A, Afdzaluddin A, Bakar MA. Electrical resistivity of Sn–3.0 Ag–0.5 Cu solder joint with the incorporation of carbon nanotubes. *Nanomaterials and Nanotechnology*. 2021 Feb; 11:1847980421996539.
- [63] Drienovsky M, Michalcová E, Pekarčíková M, Palcut M, Frolek L, Gogola P, Jančuška I, Mišík J, Gömöry F. Induction soldering of coated conductor high-temperature superconducting tapes with lead-free solder alloys. *IEEE Transactions on Applied Superconductivity*. 2018;28(4):1-5.
- [64] Dalessandro L, Odendaal WH, Kolar JW. HF characterization and nonlinear modeling of a gapped toroidal magnetic structure. *IEEE transactions on power electronics*. 2006 ;21(5):1167-75.
- [65] Mokhtari O, Nishikawa H. Correlation between microstructure and mechanical properties of Sn–Bi–X solders. *Materials Science and Engineering: A*. 2016; 651:831-9.
- [66] Zang L, Yuan Z, Zhao H, Zhang X. Wettability of molten Sn–Bi–Cu solder on Cu substrate. *Materials Letters*. 2009;63(23):2067-9.
- [67] McAlister AJ, Kahan DJ. The Al– Sn (aluminum-tin) system. *Bulletin of Alloy Phase Diagrams*. 1983;4(4):410-4.
- [68] Russell AM. Ductility in intermetallic compounds. *Advanced engineering materials*. 2003 Sep 12;5(9):629-39.
- [69] Silva BL, Spinelli JE. Correlations of microstructure and mechanical properties of the ternary Sn-9wt% Zn-2wt% Cu solder alloy. *Materials Research*. 2018;21(2).

- [70] Kim YS, Kim KS, Hwang CW, Suganuma K. Effect of composition and cooling rate on microstructure and tensile properties of Sn–Zn–Bi alloys. *Journal of alloys and compounds*. 2003;352(1-2):237-45.
- [71] Shen J, Pu Y, Yin H, Luo D, Chen J. Effects of minor Cu and Zn additions on the thermal, microstructure and tensile properties of Sn–Bi-based solder alloys. *Journal of alloys and compounds*. 2014; 614:63-70. REFalloys.
- [72] Sabri MF, Shnawah DA, Badruddin IA, Said SB, Che FX, Ariga T. Microstructural stability of Sn–1Ag–0.5 Cu–xAl (x= 1, 1.5, and 2 wt.%) solder alloys and the effects of high-temperature aging on their mechanical properties. *Materials Characterization*. 2013; 78:129-43.
- [73] Chen G, Wu F, Liu C, Xia W, Liu H. Effects of fullerenes reinforcement on the performance of 96.5 Sn–3Ag–0.5 Cu lead-free solder. *Materials Science and Engineering: A*. 2015; 636:484-92.
- [74] Gain AK, Zhang L. Temperature and humidity effects on microstructure and mechanical properties of an environmentally friendly Sn–Ag–Cu material. *Journal of Materials Science*. 2019;54(19):12863-74.
- [75] Cao X, Wang T, Ngo KD, Lu GQ. Characterization of lead-free solder and sintered nano-silver die-attach layers using thermal impedance. *IEEE Transactions on Components, Packaging and Manufacturing Technology*. 2011;1(4):495-501.
- [76] Zhao G, Wei Z, Du J, Liu W, Wang X, Yao Y. Additive manufacturing of Sn63Pb37 component by micro-coating. *Procedia Engineering*. 2016; 157:193-9.
- [77] Shi XQ, Zhou W, Pang HL, Wang ZP. Effect of temperature and strain rate on mechanical properties of 63Sn/37Pb solder alloy. *Journal of Electronic Packaging*. 1999; 121(3): 179-185.
- [78] Zhao G, Wei Z, Du J, Geng R, Xu S. Mechanical properties of Sn63Pb37 components by fused coating technology. *Additive Manufacturing*. 2018; 22:388-93.
- [79] Bonanos N, Pissis P, Macdonald JR. Impedance spectroscopy of dielectrics and electronic conductors. *Characterization of materials*. 2002:1-4.
- [80] Loyau V, Wang GY, Bue ML, Mazaleyrat F. An analysis of Mn-Zn ferrite microstructure by impedance spectroscopy, scanning transmission electron microscopy and energy dispersion spectrometry characterizations. *Journal of Applied Physics*. 2012;111(5):053928.
- [81] Steinhögl W, Schindler G, Steinlesberger G, Traving M, Engelhardt M. Comprehensive study of the resistivity of copper wires with lateral dimensions of 100 nm and smaller. *Journal of Applied Physics*. 2005;97(2):023706.

- [82] Ferreira NM, Rasekh S, Costa FM, Madre MA, Sotelo A, Diez JC, Torres MA. New method to improve the grain alignment and performance of thermoelectric ceramics. *Materials Letters*. 2012; 83:144-7.
- [83] Lormand G. Electrical properties of grain boundaries. *Le Journal de Physique Colloques*. 1982;43(C6):C6-283.
- [84] Lee WB, Bang KS, Jung SB. Effects of intermetallic compound on the electrical and mechanical properties of friction welded Cu/Al bimetallic joints during annealing. *Journal of Alloys and Compounds*. 2005;390(1-2):212-9.
- [85] Mudinepalli VR, Feng L, Lin WC, Murty BS. Effect of grain size on dielectric and ferroelectric properties of nanostructured Ba_{0.8}Sr_{0.2}TiO₃ ceramics. *Journal of Advanced Ceramics*. 2015;4(1):46-53.
- [86] Hong YK, Lee J. Ferrites for RF passive devices. In *Solid State Physics 2013 Jan 1* (Vol. 64, pp. 237-329). Academic Press.
- [87] Ashcroft N and Mermin N. *Solid State Physics*. Philadelphia: W.B. Saunders Company: 1976
- [88] Kittel C. *Introduction to Solid State Physics*. New York: Wiley: 2004
- [89] Plevachuk Y, Sklyarchuk V, Yakymovych A, Svec P, Janickovic D, Illekova E. Thermophysical properties of liquid silver-bismuth-tin alloys. *Journal of materials engineering and performance*. 2012;21(5):585-9.

Appendix A

Characterization of Traditional Lead Solder with Compositional Variation

A.1 Background

In this chapter a complete electromechanical analysis on conventional lead-tin alloys at various compositions has been performed. The purpose of the current investigation is to investigate the role that lead plays on the properties of such alloys and whether or not the use of lead in such systems can be lowered. Same methods as used in the previous sections has been used for analysis in this case.

A.2 Mechanical Characterization

Fig. A2(a) shows the ultimate tensile strength for all the samples. Interestingly the strength is higher for the alloys compared to the constituting components. Sn63Pb37 has the highest strength with the 80-20 and 50-50 following respectively. The alloy samples are followed by tin and finally lead in terms of strength. These behaviors can be justified by looking at their crystal structure.

The Strength of a metal depends on primarily on its grain size and grain boundary area. The sn80Pb20 and Sn50Pb50 alloys have two distinct structures. One being eutectic α -Pb and β -Sn layers, other being α -Pb/ β -Sn lumps. The eutectic zones have smaller grain sizes, hence more grain boundary area compared to the pure tin and lead samples which help in resisting dislocations from propagating, leading to a considerable increase in strength. The eutectic composition naturally has the highest strength. Also, in the non-eutectic lead/tin phase there will be some diffusion of Sn/Pb atoms further enhancing the alloy's strength.

In Fig. A2(b) the elongation of the materials is compared. Elongation values for the most part follow expected trend except for the 50/50 composition. Excluding the 50/50 composition, the eutectic 63/37 composition has the lowest elongation due to the presence of laminate eutectic structure. The 80/20 composition has the highest elongation. The 50/50 Lead-tin alloy has large-lead rich phases which also reduces the elongation characteristics. The elongation of the 80/20 alloy is different in this regard, indicating that the increase of the much more ductile tin-rich phase influences its ductility.

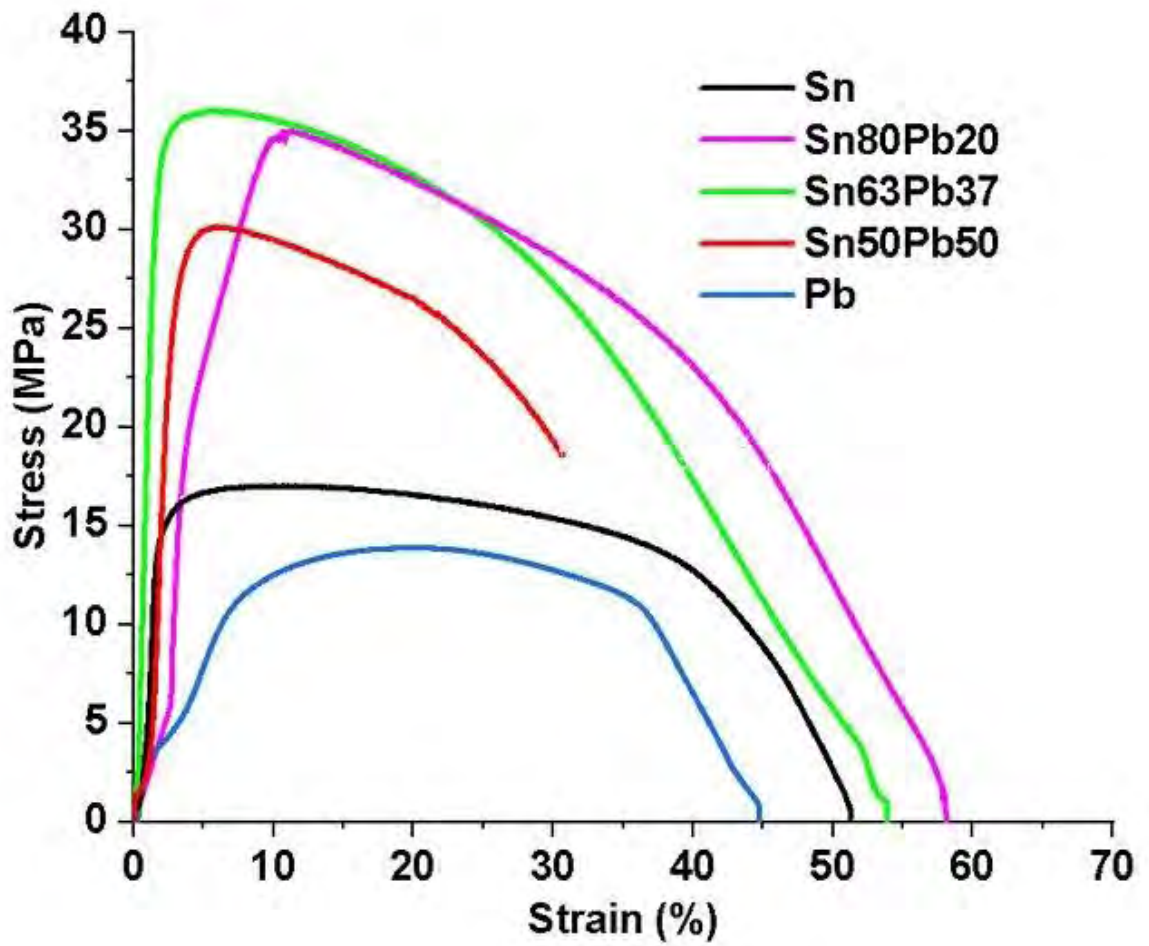


Figure A1 Stress~Strain behaviour of the alloys and constituents of lead solder

(a)

(b)

Figure A2 Mechanical characterization of Sn, Pb and Sn-Pb alloy: (a) Tensile strength, (b) Elongation

From the Fig. A3(a) it can be seen that the microhardness for the alloys exceed that of their constituents. Once again, the improved hardness of the alloys is due to their microstructures. The increased grain boundary area of the eutectic phase resists local deformation giving rise to better hardness, helping the alloys to have better hardens. 63/37 composition has the most amount of eutectic phase present, hence it has the highest hardness. The other two alloys are fairly equally spaced from the eutectic composition, hence show similar hardness. Pure lead and pure tin have much coarse grains with lower boundary area, meaning the indentation is able to propagate much more throughout the material. Lead in this regard has much rougher microstructure leading to its severely low microhardness.

Finally, Fig. A3(b) highlights the notch toughness of the four specimens. As expected, the energies, for the most part, follow the trend for the elongation at break. The 80/20 composition has the greatest energy absorption followed by the 63/37, pure tin, the 50/50 composition and pure lead respectively. However, an interesting phenomenon is observed for the lead sample. Though pure lead has fairly high ductility, the energy absorbed by it is less when compared to the other specimens. This indicates that for lead brittle intergranular fracture occurs due to the random and disorganized orientation and structure of its grain boundary.

(a)

(b)

Figure A3 Mechanical characterization of Sn, Pb and Sn-Pb alloys:(a) Microhardness and (b) Impact energy.

A.3 AC Electrical Characterization

Fig. A4(a) shows the variation of dielectric constant with frequency for the materials. All four of the materials exhibit a trend of decreasing constant with increasing frequency till

steady state. The dielectric constant for pure Tin is the highest followed by the alloys (80/20 and 50/50 respectively) and lastly lead. Higher dielectric constant of tin indicates that it has higher internal capacitive effects, especially at low frequencies. The reduced grain size of the alloy lowers the dielectric loss which will be later verified through microstructure observation. In this regard the 63/37 alloy shows exception. The increased grain boundaries due to the presence of increased eutectic structures in this composition increase the dielectric dispersion resulting in higher dielectric constant. Increasing frequencies has the same effect on all three of the materials. This effect is associated with the polarization and dispersion mechanisms of the materials. At lower frequencies dispersion due to electrons colliding with nucleus as well as ionic, electronic and interfacial polarizations occur simultaneously however with increasing frequencies all mechanisms involved in polarization except and dispersion, except electronic polarization don't have enough time to keep pace with the alternating electric field (the field alternating frequency exceeds the relaxation frequency of the dispersion and polarization mechanisms) and as a result the dielectric constant decreases. At steady state only, electric polarization is active and contributes in the dielectric constant. Lead reaching steady value earlier indicates that the relaxation frequency for its ionic polarization is much lower compared to the other materials.

Fig. A4(b) shows the dielectric loss for the samples. Dielectric loss is a measure of energy dissipated by the materials. From the graph it is seen that pure tin and the 63/37 composition have extremely high dielectric loss while loss for the other solder alloys is extremely low in comparison. Again, it can be observed that the loss tangent for all the materials attenuate around the same frequencies as dielectric constant while trailing slightly. This is to be expected as dielectric loss usually is high around polarization relaxation frequencies where the polarization lags behind the applied field resulting in an interaction between the electric field and polarization causing heating. The dielectric loss for the 50/50 alloy is the lowest of all the materials. This makes it ideal for electrical applications where low heat dissipation is warranted. Also, for the tin and 63/37 samples, the extremely high values of dielectric loss at lower frequencies indicate that the dielectric constant has a very large imaginary part. While for lead, Sn80Pb20 and Sn50Pb50 alloy the imaginary part is much lower in comparison. The eutectic composition has fine laminate structure and large grain boundary area hence more dispersion of electrons occurs and as a result the 63/37 shows high loss characteristics. Pure tin has larger grains

and a more pronounced wide grain boundary region which also causes electron scattering hence it also shows extremely high loss characteristics. The reason as to why these two alloys show the least loss is due to the grain size refinement which will be later verified by microstructure observations. From the 80/20 and 50/50 compositions it can also be seen that increasing tin phase increases the dielectric loss.

Fig. A5 illustrates the changes in the impedance of the materials as a function of frequency. The impedance of all the specimens shows a decreasing trend with frequency. The lowest impedance is that of the pure lead sample followed by the 50/50 alloy, 80/20 and 63/37 alloy respectively. Pure tin has the highest impedance.

Owing to the presence of ionic, interfacial, and electronic polarization, capacitive effects are very strong at lower frequencies. Since the capacitive and purely resistive effects are combined, this results in high impedance at lower frequencies. As field frequencies increase, the capacitive effect decreases as ionic polarization gradually fades. The capacitive effect decreases as the frequency is increased, as ionic polarization gradually fades due to field frequencies exceeding relaxation frequencies. Only the electrode's pure resistive effect remains. The impedance is reduced to a constant as a result. The presence of lead significantly lowers the impedance characteristics for the 80/20, 63/37 and 50/50 alloys.

(a)

(b)

Figure A4 AC Electrical characterization of Sn, Pb and Sn-Pb alloys: (a) Dielectric constant and (b) Dielectric loss vs frequency.

Figure A5 Relative impedance vs frequency plots for Sn, Sn80Pb20, Sn50Pb50 and Pb samples

Figure A6 DC electrical conductivity for Sn, Sn80Pb20, Sn50Pb50 and Pb samples

A.4 Bulk Conductivity

From fig. A6 it can be seen that Sn has the highest electric conductivity followed by 80/20, 50/20, 63/37 and lead respectively. Tin has a higher conductivity because its grains are more aligned. Pure lead, on the other hand, has a greater degree of grain misalignment, resulting in further electron scattering. As compared to lead, the presence of the more ordered eutectic phase gives 80/20 and 50/50 their enhanced conductivity, while the pure lead phase has the opposite effect. The grain boundary area is very high in the 63/37 composition, and as a result, it has the second worst conductive characteristics. An interesting phenomenon to note is that, despite having the best DC conductive behaviour, tin has the highest AC impedance plot. This means that in AC applications, its capacitive effects greatly outweigh its normal resistance, as impedance is the combination of a material's reactance and DC resistance.

A.5 AC Magnetic Characterization

Magnetic permeability entirely depends on the atomic structure of a material, in this regard it has almost zero relation to microstructure. Especially here where it can be observed that there is relaxation type behaviour for all the alloys. All the alloys and pure metals have very low values of real permeability indicating that they do not help with the formation of flux lines inside them under the influence of external field, especially the 80/20 composition shows best behaviour in this regard. The imaginary part of the permeability indicates the loss characteristics of a material. Higher values of imaginary part indicate more energy lost in the form of heat. Here too the Sn80Pb20 alloy shows the best characteristics.

(a)

(b)

Figure A7 AC permeability for Sn, Sn80Pb20, Sn50Pb50 and Pb samples (a) Real part
(b)Imaginary Part

A.6 Microstructure Observations

Photomicrographs of tin, alloy, and lead samples are shown in Figure A8. Tin and lead have similar microstructures, with tin having larger coarse grains with less grain boundaries but thicker grain boundaries, and lead having the worst microstructure with broken grains. Due to the presence of eutectic tin-lead phases, the grain size of the 80/20, 63/37, and 50/50 alloys is far smaller than that of their constituents. As a result, they have more room for grain boundaries. Lead's grain boundary orientation and grain alignment are the worst, resulting in lower conductivity, as previously reported.

The alternating tin-lead phase is what gives the alloys its improved strength and microhardness as well as reduced elongation at break for the 50/50 alloy specifically. This is because of the increased grain boundary area resists dislocation. While the presence of the lead phase is what ultimately helps to reduce ac impedance, dielectric loss and constant compared to pure tin. Another thing to note is that the grain size for tin is much larger than that of the other two specimens with very prominent and grain boundaries. This is the reason as to why the dielectric properties of tin is the worst of all the samples.

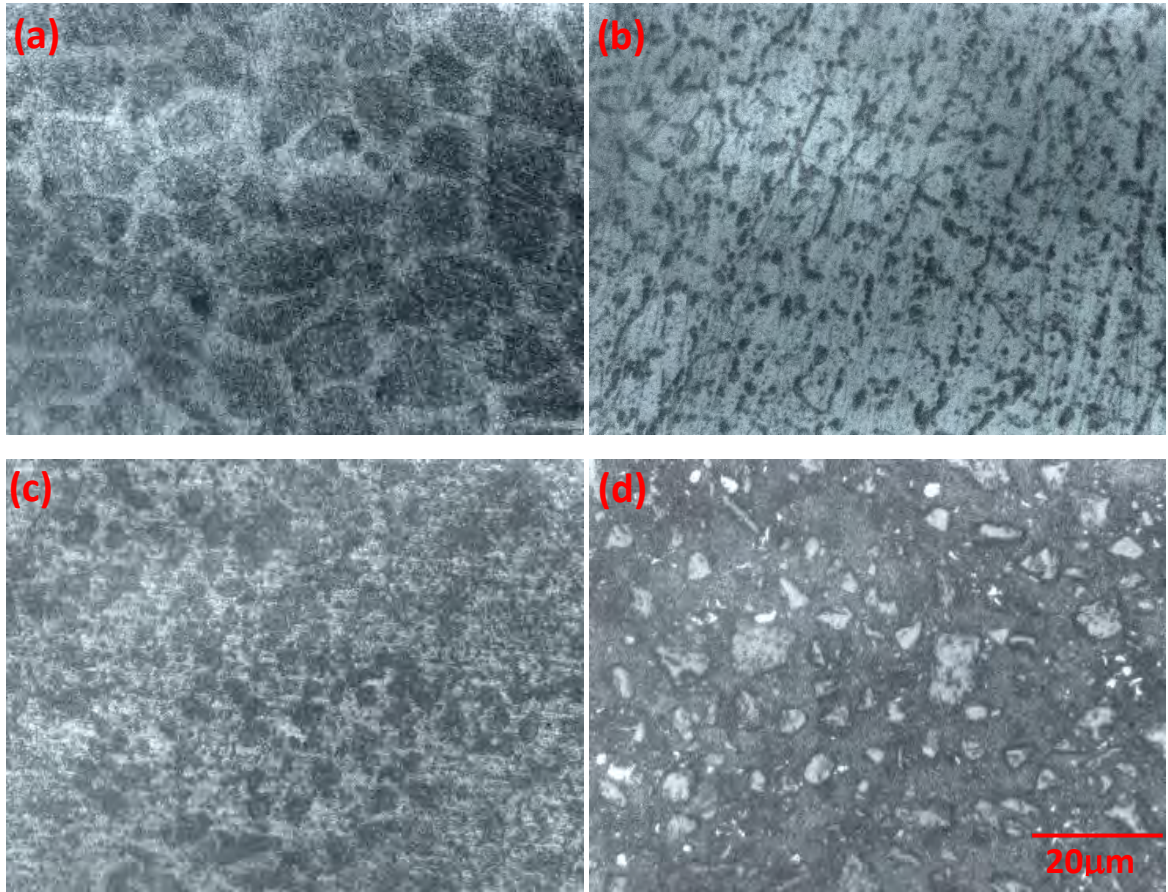


Figure A8 Optical micrograph of (a) Sn (b) Sn80-Pb20, (c) Sn50Pb50 and (d) Pb surfaces